

# Astrophysical weak-interaction rates for selected $A = 20$ and $A = 24$ nuclei

G. Martínez-Pinedo,<sup>1,2</sup> Y. H. Lam,<sup>1</sup> K. Langanke,<sup>2,1,3</sup> R. G. T. Zegers,<sup>4,5,6</sup> and C. Sullivan<sup>4,5,6</sup>

<sup>1</sup>*Institut für Kernphysik (Theoriezentrum), Technische Universität Darmstadt,  
Schlossgartenstraße 2, 64289 Darmstadt, Germany*

<sup>2</sup>*GSI Helmholtzzentrum für Schwerionenforschung, Planckstraße 1, 64291 Darmstadt, Germany*

<sup>3</sup>*Frankfurt Institute for Advanced Studies, Ruth Moufang Str. 1, D-60438 Frankfurt, Germany*

<sup>4</sup>*National Superconducting Cyclotron Laboratory, Michigan State University, East Lansing, Michigan 48824, USA*

<sup>5</sup>*Department of Physics and Astronomy, Michigan State University, East Lansing, Michigan 48824, USA*

<sup>6</sup>*Joint Institute for Nuclear Astrophysics, Michigan State University, East Lansing, Michigan 48824, USA*

(Dated: February 28, 2022)

We have evaluated the electron capture rates on  $^{20}\text{Ne}$ ,  $^{20}\text{F}$ ,  $^{24}\text{Mg}$ ,  $^{24}\text{Na}$  and the  $\beta$  decay rates for  $^{20}\text{F}$  and  $^{24}\text{Na}$  at temperature and density conditions relevant for the late-evolution stages of stars with  $M = 8\text{--}12 M_{\odot}$ . The rates are based on recent experimental data and large-scale shell model calculations. We show that the electron capture rates on  $^{20}\text{Ne}$ ,  $^{24}\text{Mg}$  and the  $^{20}\text{F}$ ,  $^{24}\text{Na}$   $\beta$ -decay rates are based on data in this astrophysical range, except for the capture rate on  $^{20}\text{Ne}$ , which we predict to have a dominating contribution from the second-forbidden transition between the  $^{20}\text{Ne}$  and  $^{20}\text{F}$  ground states in the density range  $\log \rho Y_e (\text{g cm}^{-3}) = 9.3\text{--}9.6$ . The dominance of a few individual transitions allows us to present the various rates by analytical expressions at the relevant astrophysical conditions. We also derive the screening corrections to the rates.

PACS numbers: 23.40.-s, 26.50.+x, 26.30.Jk, 21.60.Cs

## I. INTRODUCTION

Electron captures on nuclei play a crucial role in the high-density environment of late-stage stellar evolution [1, 2] with three important consequences. It reduces the pressure which the degenerate relativistic electron gas can supply against the gravitational contraction of the stellar core. Furthermore it cools the core environment as the neutrinos produced in the capture process can leave the star virtually unhindered (as long as the density is less than about  $10^{11} \text{ g cm}^{-3}$  and carry away energy. Finally electron captures change protons in the nucleus into neutrons and hence drive the stellar composition more neutron rich.

Improving on the pioneering work by Fuller, Fowler and Newman (FFN) [3, 4] and making use of advances in nuclear modeling and in computational hard- and software development, electron capture rates have been determined for sd-shell nuclei ( $A = 17\text{--}39$ ) [5] and for pf-shell nuclei ( $A = 45\text{--}64$ ) [6–8] based on large-scale shell-model diagonalization calculations. The reliability of the calculations benefitted also strongly from experimental data for the Gamow-Teller ( $\text{GT}_+$ ) distribution in nuclei (e.g. [9–11]) which determine the electron capture rates at the stellar conditions for which nuclei in the mass range  $A = 17\text{--}64$  dominate the stellar matter composition. Indeed a detailed comparison of stellar capture rates derived from experimental  $\text{GT}_+$  distributions for all  $pf$ -shell nuclei, for which data exist, with modern shell-model rates convincingly validated the use of the latter in late-stage stellar evolution studies [12] (for applications and consequences see [13]). We note that diagonalization shell-model calculations are yet not globally feasible for the very neutron-rich nuclei with  $A > 64$  which dominate the electron capture at densities in ex-

cess of a few  $10^{10} \text{ g cm}^{-3}$  [14] and the respective rates must be determined based on other approaches such as the Random Phase Approximation (RPA) with occupation numbers from Shell Monte Carlo [15], thermofield dynamics approach [16], and finite-temperature Quasi-particle RPA [17, 18].

While stellar electron captures usually occur on an ensemble of nuclei present in the matter composition, capture on the specific nuclei  $^{20}\text{Ne}$  and  $^{24}\text{Mg}$  has been identified as crucial for the core collapse of  $8\text{--}12 M_{\odot}$  stars [19, 20]. Stars in this mass range develop degenerate ONe or ONeMg cores which are driven towards collapse in a process dubbed electron capture supernova triggered by the loss of electron pressure support due to electron captures, mainly on the very abundant nuclear species  $^{20}\text{Ne}$  and  $^{24}\text{Mg}$  [19–21]. We note that  $8\text{--}12 M_{\odot}$  stars crucially contribute to the nucleosynthesis of specific nuclides. Its role for the synthesis of r-process elements is currently controversially discussed [22, 23].

Simulations of late-stage evolution of  $8\text{--}12 M_{\odot}$  stars and electron-capture supernovae usually adopt the weak-interaction rates, including those for electron capture on  $^{20}\text{Ne}$  and  $^{24}\text{Mg}$ , from the work of Oda *et al.* [5]. These authors made available rate tabulations for an extensive set of nuclei in the mass range  $A = 17\text{--}39$ , however, on a rather sparse temperature-density grid which is argued to be insufficient for detailed studies of the evolution stage for which the weak rates are essential [24]. Shell-model rates for electron captures on  $^{20}\text{Ne}$  and  $^{24}\text{Mg}$  had previously to the work by Oda *et al.* [5] been calculated by Takahara *et al.* [25]. Importantly the calculations of Takahara *et al.* and of Oda *et al.* had been performed before the Gamow-Teller strength distributions for  $^{20}\text{Ne}$  and  $^{24}\text{Mg}$  have been determined by charge-exchange experiments. Due to the isospin symmetry of the two nu-

clei, this goal could not only be achieved by techniques which determine the  $GT_+$  strength distribution using ( $d, ^2\text{He}$ ) and ( $t, ^3\text{He}$ ) reactions, but also by those measuring the  $GT_-$  distribution by ( $p, n$ ) and ( $^3\text{He}, t$ ) reactions. (In the latter a neutron is changed into a proton supplying the information required for  $\beta^-$  decays). The availability of these data calls for a reevaluation of the electron capture rates which we will present in this manuscript.

Besides the incorporation of recent experimental  $GT_+$  data, we improve the previous rates also in two other important aspects. At first we point to the relevance of the ground-state-to-ground-state transition in the capture on  $^{20}\text{Ne}$  which, although it is of forbidden nature, is likely to dominate the capture rate in the astrophysically relevant temperature-density range for the core evolution of 8-12  $M_\odot$  stars. Secondly, we correct the capture rates for screening effects in the dense environment (which decrease electron capture rates, but increase the competing  $\beta$ -decays). Our study is completed by a reevaluation of the rates for electron captures and  $\beta$  decays of  $^{20}\text{F}$  and  $^{24}\text{Na}$ , which are the daughters of the electron capture processes on  $^{20}\text{Ne}$  and  $^{24}\text{Mg}$ , respectively.

We note that the electron capture rate on  $^{20}\text{Ne}$  as well as the  $^{20}\text{F}$   $\beta$ -decay rate is dominated by a few transitions which are experimentally determined, except for the forbidden ground-state-to-ground-state transition for which only an upper limit is known. The dominance of a few transitions allows us to present the rates by an analytical expression for the relevant temperature-density region which removes uncertainties associated with extrapolations required for rate tabulations provided on a grid.

## II. FORMALISM

### A. Rates for electron capture, $\beta$ decay and neutrino energy loss

We are interested in electron capture and  $\beta^-$  decay rates for temperatures  $T = 10^8$ – $10^{10}$  K and densities  $\rho = 10^8$ – $10^{10}$  g  $\text{cm}^{-3}$ . Under these conditions nuclei are fully ionized and the electrons form a degenerate relativistic Fermi gas. Hence the rate formalism as derived by Fuller *et al.* applies [3, 4] which we summarize in the following.

The total rate for electron capture and  $\beta^-$  decay is given by

$$\lambda^\alpha = \frac{1}{G(Z, A, T)} \sum_{if} (2J_i + 1) \lambda_{if}^\alpha e^{-E_i/(kT)}, \quad (1)$$

where the sums in  $i$  and  $f$  run over states in the parent and daughter nuclei, respectively, and the superscript  $\alpha$  stands for electron capture (ec) or  $\beta^-$ -decay.  $G(Z, A, T) = \sum_i (2J_i + 1) \exp(-E_i/(kT))$  is the partition function of the parent nucleus. The electron capture rate from state  $i$  to state  $f$  is given by:

$$\lambda_{if}^{\text{ec}} = \frac{\ln 2}{K} B_{if} \Phi^{\text{ec}}(q_{if}), \quad (2a)$$

$$\Phi^{\text{ec}}(q_{if}) = \int_{w_l}^{\infty} w p(q_{if} + w)^2 F(Z, w) S_e(w) dw; \quad (2b)$$

while for  $\beta^-$ -decay we have:

$$\lambda_{if}^{\beta^-} = \frac{\ln 2}{K} B_{if} \Phi^\beta(q_{if}), \quad (3a)$$

$$\Phi^\beta(q_{if}) = \int_1^{q_{if}} w p(q_{if} - w)^2 F(Z + 1, w) (1 - S_e(w)) dw. \quad (3b)$$

The constant  $K$  can be determined from superallowed Fermi transitions and we used  $K = 6144 \pm 2$  s [26].  $w$  is the total, rest mass plus kinetic, energy of the electron in units of  $m_e c^2$ , and  $p = \sqrt{w^2 - 1}$  is the electron momentum in units of  $m_e c$ . We have introduced the energy difference between initial and final nuclear states,  $q_{if}$ , in units of  $m_e c^2$

$$q_{if} = \frac{Q_{if}}{m_e c^2}, \quad Q_{if} = (M_p c^2 - M_d c^2 + E_i - E_f), \quad (4)$$

where  $M_p$ ,  $M_d$  are the nuclear masses of the parent and daughter nucleus, respectively, while  $E_i$ ,  $E_f$  are the excitation energies of the initial and final states. We have calculated the nuclear masses from the tabulated atomic masses neglecting atomic binding energies.  $w_l$  is the capture threshold total energy, rest plus kinetic, in units of  $m_e c^2$  for electron capture. Depending on the value of  $q_{if}$  one has  $w_l = 1$  if  $q_{if} > -1$ , or  $w_l = |q_{if}|$  if  $q_{if} < -1$ .  $S_e$  is the electron distribution function, which for the stellar conditions, we are interested in, is given by a Fermi-Dirac distribution with temperature  $T$  and chemical potential  $\mu_e$ ,

$$S_e(E_e) = \frac{1}{\exp\left(\frac{E_e - \mu_e}{kT}\right) + 1}, \quad (5)$$

with  $E_e = w m_e c^2$ . The chemical potential,  $\mu_e$ , is determined from the density inverting the relation

$$\rho Y_e = \frac{m_u}{\pi^2} \left(\frac{m_e c}{\hbar}\right)^3 \int_0^\infty (S_e - S_p) p^2 dp, \quad (6)$$

where  $m_u$  is the atomic mass unit and  $S_p$  is the positron distribution which is obtained from  $S_e$  by the replacement  $\mu_p = -\mu_e$ . Note that the density of electron-positron pairs has been removed in (6) by forming the difference  $S_e - S_p$ .

Finally,  $B_{if}$  is the reduced transition probability of the nuclear transition. Except for the forbidden ground-state-to-ground-state transition in  $^{20}\text{Ne}$  we will only consider GT contributions:

$$B_{if} = B_{if}(GT) = g_A^2 \frac{\langle f || \sum_k \boldsymbol{\sigma}^k \mathbf{t}_{\pm}^k || i \rangle^2}{2J_i + 1}. \quad (7)$$

Here the matrix element is reduced with respect to the spin operator  $\boldsymbol{\sigma}$  only (Racah convention [27]) and the sum runs over all nucleons. For the isospin operators,  $\mathbf{t}_{\pm} = (\boldsymbol{\tau}_x \pm i\boldsymbol{\tau}_y)/2$ , we use the convention  $\mathbf{t}_{+p} = n$ ; thus, ‘+’ refers to electron capture and ‘-’ to  $\beta^-$  transitions.  $g_A$  is the weak axial coupling constant,  $g_A = -1.26$ . When using theoretical Gamow-Teller matrix elements we use an effective coupling constant  $g_A^{\text{eff}} = 0.74g_A$  to account for the observed quenching of the GT strength in shell model calculations [28–31].

The remaining factor appearing in the phase space integrals is the Fermi function,  $F(Z, w)$ , that corrects the phase space integral for the Coulomb distortion of the electron wave function near the nucleus.

In astrophysical applications, in addition of the weak interaction rates one is also interested in the energy loss by neutrino emission. This can be determined by including an additional power of the neutrino energy in equations (2) and (3). In this case the total neutrino energy loss rate becomes:

$$\xi^{\alpha} = \frac{1}{G(Z, A, T)} \sum_{if} (2J_i + 1) \xi_{if}^{\alpha} e^{-E_i/(kT)}, \quad (8)$$

and for the neutrino energy loss due to electron capture from state  $i$  to state  $f$  we have:

$$\xi_{if}^{\text{ec}} = \frac{(\ln 2)m_e c^2}{K} B_{if} \Psi^{\text{ec}}(q_{if}), \quad (9a)$$

$$\Psi^{\text{ec}}(q_{if}) = \int_{w_1}^{\infty} wp(q_{if} + w)^3 F(Z, w) S_e(w) dw; \quad (9b)$$

while for  $\beta^-$ -decay we have:

$$\xi_{if}^{\beta^-} = \frac{(\ln 2)m_e c^2}{K} B_{if} \Psi^{\beta}(q_{if}), \quad (10a)$$

$$\Psi^{\beta}(q_{if}) = \int_1^{q_{if}} wp(q_{if} - w)^3 F(Z + 1, w) (1 - S_e(w)) dw. \quad (10b)$$

Similarly one can compute the average energy of the emitted neutrino by the ratio:

$$\langle E_{\nu} \rangle^{\alpha} = \frac{\xi^{\alpha}}{\lambda^{\alpha}} \quad (11)$$

where  $\alpha$  stands for either electron capture or beta-decay.

## B. Approximate expressions

The evaluation of electron capture and beta-decay rates requires the calculation of the phase space integrals appearing in equations (2), (3), (9) and (10). These integrals make the rates extremely sensitive to variations of temperature and density. As weak interaction rate tabulations [3, 5, 8] are normally provided on a grid of densities and temperatures, this requires the development of accurate interpolation schemes between the grid points at which the rates have been evaluated. For the high temperature ( $T > 10^9$  K) and density conditions relevant for presupernova evolution [32], many transitions from both the initial and final nucleus contribute to the sum in equation (1) and the density and temperature dependence of the rates can well be approximated by an effective phase space integral,  $\Phi_e^{\text{ec}}$ , corresponding to the ground-state to ground-state transition. This allows to introduce an effective  $\langle ft \rangle$  value that is expected to be almost constant over a large range of temperature and densities [4]:

$$\lambda^{\text{ec}} = \ln 2 \frac{\Phi_e^{\text{ec}}}{\langle ft \rangle}. \quad (12)$$

In the present work, we are interested in conditions for which URCA processes operate in both intermediate mass stars [33] and neutron star crust [34]. This corresponds to temperatures in the range  $10^8$ – $10^9$  K for which, in contrast to the presupernova conditions, both electron capture and beta-decay rates are determined by a few transitions (see section III) with very different phase space dependencies. The application of the above approach will result in changes in the effective  $\langle ft \rangle$  value of several orders of magnitude when the rate changes from being dominated by one transition to another transition. As this occurs in a very narrow density range, it makes it impractical to use the effective  $\langle ft \rangle$  formalism for the rate interpolation. Nevertheless, one can still use the fact that the rates are determined by a few transitions to provide accurate analytic expressions for the relevant rates. This constitutes a generalization of the FFN effective  $\langle ft \rangle$  formalism and its extension to beta-decay rates.

In the evaluation of the phase space integral in equation (12) one can use the fact that for the large electron energies involved the Fermi function,  $F(Z, w)$ , can be approximated up to a constant factor (which can be subsumed in a redefinition of the matrix element) by the ratio  $w/p$ :

$$\Phi_e^{\text{ec}}(Q, T, \mu_e) = \int_{w_1}^{\infty} w^2 (q + w)^2 S_e(w) dw, \quad (13)$$

where we have made explicit the dependence of the integral on temperature, electron chemical potential,  $\mu_e$ , and  $Q$ -value for the ground-state to ground-state transition,  $Q = qm_e c^2$ .  $\Phi_e^{\text{ec}}$  can be expressed as a combination of relativistic Fermi integrals (or equivalently polylogarithmic

functions, Li):

$$F_k(\eta) = \int_0^\infty \frac{x^k}{\exp(x - \eta) + 1} dx, \quad (14)$$

$$F_k(\eta) = -\Gamma(k + 1)\text{Li}_{k+1}(-e^\eta);$$

to obtain

$$\Phi_e^{\text{ec}}(Q, T, \mu_e) = \left(\frac{kT}{m_e c^2}\right)^5 [F_4(\eta) - 2\chi F_3(\eta) + \chi^2 F_2(\eta)] \quad (15)$$

with  $\eta = (\mu_e + Q)/(kT)$ ,  $\chi = Q/(kT)$ , and we have assumed that  $Q < -m_e c^2$ , which is the case for all the nuclei considered here. For the evaluation of the Fermi functions appearing in equation (15) one can use several publicly available numerical routines both in C [35] and in Fortran [36, 37]. Alternatively, Fuller *et al.* [4] developed approximations for the Fermi functions that are valid for  $\eta \ll 0$  and  $\eta \gg 0$  and reproduce the exact results with an accuracy of better than 20% around  $\eta \approx 0$ :

$$F_0(\eta) = \ln(1 + e^\eta); \quad (16a)$$

$$F_1(\eta) = \begin{cases} e^\eta & \eta \leq 0, \\ \frac{1}{2}\eta^2 + 2 - e^{-\eta} & \eta > 0; \end{cases} \quad (16b)$$

$$F_2(\eta) = \begin{cases} 2e^\eta & \eta \leq 0, \\ \frac{1}{3}\eta^3 + 4\eta + 2e^{-\eta} & \eta > 0; \end{cases} \quad (16c)$$

$$F_3(\eta) = \begin{cases} 6e^\eta & \eta \leq 0, \\ \frac{1}{4}\eta^4 + \frac{\pi^2}{2}\eta^2 + 12 - 6e^{-\eta} & \eta > 0; \end{cases} \quad (16d)$$

$$F_4(\eta) = \begin{cases} 24e^\eta & \eta \leq 0, \\ \frac{1}{5}\eta^5 + \frac{2\pi^2}{3}\eta^3 + 48\eta + 24e^{-\eta} & \eta > 0; \end{cases} \quad (16e)$$

$$F_5(\eta) = \begin{cases} 120e^\eta & \eta \leq 0, \\ \frac{1}{6}\eta^6 + \frac{5\pi^2}{6}\eta^4 + \frac{7\pi^4}{6}\eta^2 + 240 - 120e^{-\eta} & \eta > 0; \end{cases} \quad (16f)$$

where we have included the expressions for  $F_0(\eta)$  and  $F_1(\eta)$  that are necessary for the beta-decay rates and corrected for a typo in the approximation of  $F_5(\eta)$  in ref. [4].

The partial contribution to the total electron capture rate of an initial state,  $i$ , with excitation energy  $E_i$  and angular momentum  $J_i$  to a final state,  $f$ , with excitation energy  $E_f$  and angular momentum  $J_f$  can be expressed as:

$$\Lambda_{if}^{\text{ec}} = (2J_i + 1)e^{-E_i/(kT)} \lambda_{if}^{\text{ec}} = \frac{(\ln 2)B_{if}^e}{K} (2J_i + 1)e^{-E_i/(kT)} \Phi_e^{\text{ec}}(Q_{if}, T, \mu_e) \quad (17)$$

with  $Q_{if} = Q + E_i - E_f$ . During the early evolution of an ONeMg core the electron chemical potential,  $\mu_e$ , is typically much smaller than the magnitude of the capture  $Q$ -value,  $|Q_{if}|$ , i.e.  $\eta \ll 0$ . Under these conditions the

Fermi integrals appearing in (15) can be approximated as  $F_k(\eta) \approx k!e^\eta$ . Keeping the leading terms in eq. (17) we obtain:

$$\Lambda_{if}^{\text{ec}} = \frac{(\ln 2)B_{if}^e}{K} \left(\frac{kT}{m_e c^2}\right)^5 2(2J_i + 1) \left(\frac{Q + E_i - E_f}{kT}\right)^2 \exp\left(\frac{Q - E_f + \mu_e}{kT}\right) \quad (18)$$

One can see that the exponential dependence on the excitation energy of the initial state has disappeared. The physical reason is that with increasing excitation energy the exponential decrease in the thermal probability of populating an excited state is exactly compensated by the exponential increase in the number of electrons that can contribute to the capture process. Under these conditions the rate grows exponentially with increasing electron chemical potential. This increase holds as long as

$\mu_e \ll -Q_{if}$  and  $E_i \ll -Q$ . Once the chemical potential  $\mu_e$  becomes larger than the absolute  $Q$ -value, the Fermi integrals can be approximated as  $F_k(\eta) \approx \eta^{k+1}/(k+1)$ . It is interesting to consider two possible limits, i) the electron fermi energy is similar to the capture  $Q$ -value,  $\mu_e \approx |Q_{if}|$  and ii) the electron fermi energy is much larger than the capture  $Q$ -value,  $\mu_e \gg |Q_{if}|$ . In the first case we obtain

$$\Lambda_{if}^{\text{ec}} = \frac{(\ln 2)B_{if}^e}{3K}(2J_i + 1) \exp\left(-\frac{E_i}{kT}\right) \frac{(Q + E_i - E_f)^2(\mu_e + Q + E_i - E_f)^3}{(m_e c^2)^5}, \quad (19)$$

while for the second

$$\Lambda_{if}^{\text{ec}} = \frac{(\ln 2)B_{if}^e}{5K}(2J_i + 1) \exp\left(-\frac{E_i}{kT}\right) \left(\frac{\mu_e + Q + E_i - E_f}{m_e c^2}\right)^5. \quad (20)$$

Under these conditions the contribution of excited states is exponentially suppressed and the capture rate on each state is almost independent of the temperature.

Similar approximations can be obtained for the neutrino energy loss rate. The contribution of a transition from an initial state  $i$  to a final state  $f$  is then given by:

$$\Xi_{if}^{\text{ec}} = (2J_i + 1)\xi_{if}^\alpha e^{-E_i/(kT)} = \frac{(\ln 2)B_{if}^e}{K} m_e c^2 (2J_i + 1) e^{-E_i/(kT)} \Psi_e^{\text{ec}}(Q_{if}, T, \mu_e) \quad (21)$$

with

$$\Psi_e^{\text{ec}}(Q, T, \mu_e) = \left(\frac{kT}{m_e c^2}\right)^6 [F_5(\eta) - 2\chi F_4(\eta) + \chi^2 F_3(\eta)], \quad (22)$$

and  $\eta = (\mu_e + Q)/(kT)$ ,  $\chi = Q/(kT)$ .

Again we can obtain approximate expressions for the limiting cases  $\mu_e \ll -Q_{if}$ :

$$\Xi_{if}^{\text{ec}} = \frac{(\ln 2)B_{if}^e}{K} \frac{(kT)^6}{(m_e c^2)^5} 6(2J_i + 1) \left(\frac{Q + E_i - E_f}{kT}\right)^2 \exp\left(\frac{Q - E_f + \mu_e}{kT}\right); \quad (23)$$

$\mu_e \approx -Q_{if}$ :

$$\Xi_{if}^{\text{ec}} = \frac{(\ln 2)B_{if}^e}{4K}(2J_i + 1) \exp\left(-\frac{E_i}{kT}\right) \frac{(Q + E_i - E_f)^2(\mu_e + Q + E_i - E_f)^4}{(m_e c^2)^5}; \quad (24)$$

and  $\mu_e \gg -Q_{if}$ :

$$\Xi_{if}^{\text{ec}} = \frac{(\ln 2)B_{if}^e}{6K}(2J_i + 1) \exp\left(-\frac{E_i}{kT}\right) \frac{(\mu_e + Q + E_i - E_f)^6}{(m_e c^2)^5}. \quad (25)$$

Combining equations (18) and (23) one obtains that the average neutrino energy for conditions  $\mu_e \ll -Q_{if}$  is:

$$\langle E_\nu \rangle^{\text{ec}} \approx 3kT \quad (26)$$

independently of the initial state on which the electron capture takes place. Similarly from equations (19) and (24) we obtain for  $\mu_e \approx -Q_{if}$ :

$$\langle E_\nu \rangle^{\text{ec}} = \frac{3}{4}(\mu_e + Q + E_i - E_f) \quad (27)$$

that agrees with the result of refs. [38] and [39] (but with

a factor 3/4 instead of 3/5). From equations (20) and (25) we obtain for  $\mu_e \gg -Q_{if}$

$$\langle E_\nu \rangle^{\text{ec}} = \frac{5}{6}(\mu_e + Q + E_i - E_f) \approx \frac{5}{6}\mu_e \quad (28)$$

recovering the well known result of refs. [39, 40].

The beta-decay rates can also be expressed as combinations of Fermi functions. For that one can approximate the phase space integral in equation (3b) by:

$$\Phi_e^\beta(Q, T, \mu_e) = \int_1^q w^2 (q-w)^2 (1 - S_e(w)) dw \quad (29)$$

with  $q = Q/(m_e c^2)$ . This can be expressed in terms of Fermi functions as:

$$\Phi_e^\beta(Q, T, \mu_e) = \left(\frac{kT}{m_e c^2}\right)^5 \left[ -\vartheta^2(\vartheta - \chi)^2 F_0(-\eta_m) + 2\vartheta(\chi^2 + 2\vartheta^2 - 3\chi\vartheta) F_1(-\eta_m) + (-\chi^2 - 6\vartheta^2 + 6\chi\vartheta) F_2(-\eta_m) \right. \\ \left. + (4\vartheta - 2\chi)F_3(-\eta_m) - F_4(-\eta_m) + \chi^2 F_2(-\eta) - 2\chi F_3(-\eta) + F_4(-\eta) \right] \quad (30)$$

with  $\vartheta = m_e c^2/(kT)$ ,  $\chi = Q/(kT)$ ,  $\eta_m = (\mu_e - m_e c^2)/(kT)$  and  $\eta = (\mu_e - Q)/(kT)$ . For the conditions we are interested in one has  $\eta_m \gg 1$ . The Fermi integrals with arguments  $-\eta_m$  behave like  $\exp(-\eta_m)$  and their contributions can be neglected. Under these conditions we obtain:

$$\Phi_e^\beta(Q, T, \mu_e) = \left(\frac{kT}{m_e c^2}\right)^5 [F_4(-\eta) - 2\chi F_3(-\eta) + \chi^2 F_2(-\eta)], \quad (31)$$

which is very similar to equation (15). In the limit where final state blocking can be neglected, i.e.  $\mu_e \ll m_e c^2$ ,

equation (30) reduces to:

$$\Phi_e^\beta(Q, T, \mu_e) \approx \frac{1}{30}(q-1)^3(6+3q+q^2) \quad (32)$$

with  $q = Q/(m_e c^2)$ . For partial blocking of the final state,  $\mu_e \lesssim Q$ , we obtain

$$\Phi_e^\beta(Q, T, \mu_e) \approx \frac{Q^2(Q - \mu_e)^3}{3(m_e c^2)^5} \quad (33)$$

In the limit of strong final state blocking, i.e.  $\mu_e \gg Q$  we get:

$$\Phi_e^\beta(Q, T, \mu_e) \approx 2 \left(\frac{kT}{m_e c^2}\right)^5 \left(\frac{Q}{kT}\right)^2 \exp\left(\frac{Q - \mu_e}{kT}\right). \quad (34)$$

For these conditions, the contribution of a transition from an initial state  $i$  to a final state  $f$  to the beta-decay rate can be expressed as:

$$\Lambda_{if}^\beta = \frac{(\ln 2)B_{if}^e}{K} \left(\frac{kT}{m_e c^2}\right)^5 2(2J_i + 1) \left(\frac{Q + E_i - E_f}{kT}\right)^2 \exp\left(\frac{Q - E_f - \mu_e}{kT}\right) \quad (35)$$

As for electron capture, the  $\beta$ -decay rate does not depend on the excitation energy of the initial state. Furthermore, the strong similarity with equation (18) is remarkable. This shows that beta-decays decrease with exactly the same exponential dependence on  $\mu_e$  as the electron

captures increase and probes the potential of equation (30) for interpolating beta-decay rates under presupernova conditions.

For the rate of neutrino energy loss by beta-decay we obtain:

$$\Psi_e^\beta(Q, T, \mu_e) = \left(\frac{kT}{m_e c^2}\right)^6 \left[ \vartheta^2(\vartheta - \chi)^3 F_0(-\eta_m) - \vartheta(5\vartheta - 2\chi)(\vartheta - \chi)^2 F_1(-\eta_m) \right. \\ \left. + (\chi^2 + 10\vartheta^2 - 8\chi\vartheta)(\vartheta - \chi)F_2(-\eta_m) - (3\chi^2 + 10\vartheta^2 - 12\chi\vartheta)F_3(-\eta_m) \right. \\ \left. + (5\vartheta - 3\chi)F_4(-\eta_m) - F_5(-\eta_m) + \chi^2 F_3(-\eta) - 2\chi F_4(-\eta) + F_5(-\eta) \right]. \quad (36)$$

For  $\eta_m \gg 1$  the expression reads

$$\Psi_e^\beta(Q, T, \mu_e) = \left(\frac{kT}{m_e c^2}\right)^6 [F_5(-\eta) - 2\chi F_4(-\eta) + \chi^2 F_3(-\eta)] \quad (37)$$

In the limit of no final state blocking, i.e.  $\mu_e \ll m_e c^2$ ,

eq. (36) reduces to:

$$\Psi_e^\beta(Q, T, \mu_e) \approx \frac{1}{60}(q-1)^4(q^2 + 4q + 10). \quad (38)$$

The average energy of the emitted neutrino becomes:

$$\langle E_\nu \rangle^\beta = m_e c^2 \frac{(q-1)(q^2+4q+10)}{2(q^2+3q+6)} \approx m_e c^2 \left( \frac{q}{2} - \frac{5}{q^2} \right). \quad (39)$$

For partial final state blocking,  $\mu_e \lesssim Q$  we get:

$$\Psi_e^\beta(Q, T, \mu_e) \approx \frac{Q^2(Q-\mu_e)^4}{4m_e c^2} \quad (40)$$

and for the average energy of the emitted neutrino:

$$\langle E_\nu \rangle^\beta = \frac{3}{4}(Q + E_i - E_f - \mu_e), \quad (41)$$

where we have explicitly recovered the dependence on the excitation energies of initial and final states to make clear the similarity with equation (27) for electron capture.

In the limit of large final state blocking, i.e.  $\mu_e \gg Q$  we obtain:

$$\Psi_e^\beta(Q, T, \mu_e) \approx 6 \left( \frac{kT}{m_e c^2} \right)^6 \left( \frac{Q}{kT} \right)^2 \exp \left( \frac{Q - \mu_e}{kT} \right) \quad (42)$$

and for the contribution to the total beta-decay rate of the transition  $i \rightarrow f$ :

$$\Xi_{if}^\beta = \frac{(\ln 2) B_{if}^e}{K} m_e c^2 \left( \frac{kT}{m_e c^2} \right)^6 6(2J_i + 1) \left( \frac{Q + E_i - E_f}{kT} \right)^2 \exp \left( \frac{Q - E_f - \mu_e}{kT} \right). \quad (43)$$

This again is remarkably similar to the equivalent expression for electron capture (23). Under these conditions the average energy of the emitted neutrino becomes:

$$\langle E_\nu \rangle^\beta = 3kT \quad (44)$$

and is independent of the particular transitions that dominate the rate.

### C. Determination of energy generation

Apart of the fact that weak interaction processes change the electron content of the star, they are also important because they can be either a source or loss of energy for the star. The neutrinos that are produced by the weak interaction leave the star carrying away part of the energy generated. However, depending on the conditions the net energy generation could still be positive or negative. From basic thermodynamics and assuming that the time scale to maintain thermodynamical equilibrium is shorter than the time scale for weak interaction processes, we obtain the following relation valid at every point of the star:

$$kT \frac{ds}{dt} + \sum_i \mu_i \frac{dY_i}{dt} = \frac{dq}{dt} \quad (45)$$

where  $s$  is the entropy per nucleon,  $\mu_i$  is the chemical potential including rest mass for species  $i$  with abundance  $Y_i$  and the sum runs over all particles including nuclei and electrons.  $dq/dt$  represents the heat per nucleon and time which is being added to or lost from the region being considered. In the case of weak processes, heat is lost by neutrinos. In the case of electron capture in a nucleus  $a$  producing a nucleus  $b$  with energy threshold  $Q_{ec} =$

$-Q_{\beta^-} = -Q$ , i.e. the ground-state to ground-state  $Q$ -value, we have:

$$kT \frac{ds}{dt} = -\frac{dY_e}{dt} (\mu_e - Q - \langle E_\nu \rangle^{ec}) - kT \frac{dY_e}{dt} \ln \left[ \frac{Y_a G_b}{Y_b G_a} \right] \quad (46)$$

while for the beta decay of nucleus  $b$  to a nucleus  $a$  we obtain

$$kT \frac{ds}{dt} = \frac{dY_e}{dt} (Q - \mu_e - \langle E_\nu \rangle^\beta) + kT \frac{dY_e}{dt} \ln \left[ \frac{Y_b G_a}{Y_a G_b} \right], \quad (47)$$

where  $Y_{a,b}$  represent the abundances of nuclei  $a, b$  and the second term in both expressions has been obtained assuming a non-interacting Boltzmann gas expression for the chemical potential of nuclei. This term is typically negligible except in the case of very different abundance of nuclei  $a$  and  $b$ .

Equations (46) and (47) show that the determination of the energy generation requires only the knowledge of the average energy of the produced neutrino and it is not necessary to compute the so-called gamma ray heating rates [5, 25], corresponding to the decay by gamma emission of excited states populated after the weak transition. This does not mean that transitions to excited states are not important. In fact, they normally have larger contributions to the energy generation [41] due to the fact that the average energy of the neutrinos is smaller. However, one has also to consider that the weak process can start in excited states and in that case the gamma heating rates can in fact be negative.

As electron captures decrease  $Y_e$ , while beta decays increase  $Y_e$ , the energy generation will be positive or negative depending on the sign of the quantity  $\mathcal{E}^{ec} = \mu_e - Q - \langle E_\nu \rangle^{ec}$  for electron capture and  $\mathcal{E}^\beta = Q - \mu_e - \langle E_\nu \rangle^\beta$  for  $\beta^-$ -decay (neglecting the second terms in Eqs. (46) and (47)). Using energy conservation to relate the energy

of the electron and the energy of the neutrino in equations (9b) and (10b) we obtain the following relations for electron capture,

$$\langle E_e \rangle^{\text{ec}} + \langle E_i \rangle^{\text{ec}} = \langle E_f \rangle^{\text{ec}} + Q + \langle E_\nu \rangle^{\text{ec}}, \quad (48)$$

and beta decay,

$$\langle E_i \rangle^\beta + Q = \langle E_f \rangle^\beta + \langle E_e \rangle^\beta + \langle E_\nu \rangle^\beta, \quad (49)$$

where  $\langle E_e \rangle^{\text{ec}}$  ( $\langle E_e \rangle^\beta$ ) is the average energy of the captured electron (emitted electron) and  $\langle E_i \rangle^{\text{ec}}$  and  $\langle E_f \rangle^{\text{ec}}$  ( $\langle E_i \rangle^\beta$  and  $\langle E_f \rangle^\beta$ ) represent the average energy of the initial and final nuclei in the electron capture ( $\beta$ -decay) process. We can define the average energy of the produced gammas as:  $\langle E_\gamma \rangle^\alpha = \langle E_f \rangle^\alpha - \langle E_i \rangle^\alpha$ , where  $\alpha$  stands for electron capture and beta decay. Notice that this quantity can be negative, meaning that transitions from excited parent nuclear states dominate the weak process and the nucleus has to absorb gamma radiation to populate these states. Combining the above expressions we obtain the following relations for the quantities  $\mathcal{E}^{\text{ec}}$  and  $\mathcal{E}^\beta$ :

$$\mathcal{E}^{\text{ec}} = \mu_e - Q - \langle E_\nu \rangle^{\text{ec}} = \mu_e - \langle E_e \rangle^{\text{ec}} + \langle E_\gamma \rangle^{\text{ec}} \quad (50a)$$

$$\mathcal{E}^\beta = Q - \mu_e - \langle E_\nu \rangle^\beta = \langle E_e \rangle^\beta + \langle E_\gamma \rangle^\beta - \mu_e \quad (50b)$$

Electron captures will be endothermic, i.e. they absorb energy, when the electron chemical potential is smaller than  $Q$ . Under these conditions  $\langle E_\nu \rangle^{\text{ec}} \approx 3kT$ , see eq (26), and  $\mathcal{E}^{\text{ec}} \approx -(Q - \mu_e + 3kT)$ . Equivalently, this means that the average energy of the captured electrons is larger than the sum of the chemical potential and gamma ray energies [42]. Under these conditions the electron capture rate is rather small and beta decay is exothermic, i.e. it generates energy, with

$$\mathcal{E}^\beta \approx \langle E_\gamma \rangle^\beta + (Q - \langle E_\gamma \rangle^\beta - \mu_e)/4 \quad (51)$$

where we have used (41) to relate the neutrino energy loss rate to the average gamma energy. Equivalently, see eq. (50b), the sum of the average energies of the electrons and gammas produced by beta decay is larger than the electron chemical potential. Under these conditions, the beta decay rate is normally much larger than the electron capture rate, however, the abundance of the beta-decaying nucleus is still rather small as very little material has been produced by electron capture.

As the electron chemical potential grows, the net energy generation in electron capture and beta-decay could be positive or negative depending on the particular temperature/density conditions and the structure of the nuclei involved.

Electron captures will be exothermic whenever the electron chemical potential becomes larger than the capture threshold. For these conditions the electron capture proceeds rapidly and the heating is large with

$$\mathcal{E}^{\text{ec}} \approx \langle E_\gamma \rangle^{\text{ec}} + (\mu_e - Q - \langle E_\gamma \rangle^{\text{ec}})/4, \quad (52)$$

where we have estimated the neutrino energy loss using eq. (27). The energy generation becomes larger the higher the average energy of the produced gammas [41], i.e. the higher the excitation energy of the final states. The electrons captured have on average energies smaller than the sum of the electron chemical potential plus the average gamma energy [43], see equation (50a). Under these conditions the beta-decay rate is rather small and its contribution to the energy generation is negligible.

### III. RESULTS

#### A. Rates for the $A = 20$ nuclei

For the study of the electron capture on  $^{20}\text{Ne}$  and the  $\beta^-$  decay of  $^{20}\text{F}$  we have adopted the following set of experimental and calculated transitions. We use the  $(p, n)$  data on  $^{20}\text{Ne}$  of [44] and assume isospin symmetry to determine the  $\text{GT}_+$  transitions from the  $^{20}\text{Ne}$  ground state to low lying excited  $1^+$  states in  $^{20}\text{F}$ . From  $^{20}\text{F}$   $\beta$  decay data [45] we determined the GT matrix element for the transition from the  $2^+$  state in  $^{20}\text{Ne}$  at  $E_x = 1.634$  MeV to the  $2^+$   $^{20}\text{F}$  ground state. We approximate the non-unique second forbidden transition from the  $2^+$  ground state in  $^{20}\text{Ne}$  to the  $2^+$  ground state in  $^{20}\text{F}$  by the upper limit obtained in the  $^{20}\text{F}$   $\beta$  data.

The experimental data were supplemented by shell model  $\text{GT}_+$  strength functions from the  $^{20}\text{Ne}$  first  $2^+$  and  $4^+$  excited states, and the backresonance transitions corresponding to the  $\text{GT}_-$  strength on the  $2^+$  ground state and the lowest  $3^+$ ,  $4^+$ ,  $1^+$ ,  $5^+$  and  $2^+$  excited states of  $^{20}\text{F}$ . The shell-model calculations were performed within the complete  $sd$ -shell using the USDB interaction [46]. We use experimental values for the excitation energies whenever they are known.

TABLE I. Information that determines the electron capture rate on  $^{20}\text{Ne}$  and beta decay of  $^{20}\text{F}$  for the relevant temperatures and densities. The ground-state to ground-state electron  $Q$ -value is  $Q_{\text{ec}} = -7.535$  MeV [47].

| Initial $^{20}\text{Ne}$ state |              | Final $^{20}\text{F}$ state |              | Matrix element                     |
|--------------------------------|--------------|-----------------------------|--------------|------------------------------------|
| $J^\pi$                        | Energy (MeV) | $J^\pi$                     | Energy (MeV) | $B$                                |
| $0^+$                          | 0            | $1^+$                       | 1.057        | 0.256                              |
| $0^+$                          | 0            | $2^+$                       | 0            | $9.72 \times 10^{-7}{}^{\text{a}}$ |
| $2^+$                          | 1.634        | $2^+$                       | 0            | 0.0659                             |
| $2^+$                          | 1.634        | $3^+$                       | 0.656        | 0.0653 <sup>b</sup>                |

<sup>a</sup> Upper experimental limit

<sup>b</sup> Theoretical value

In Fig. 1 we plot our calculated  $^{20}\text{Ne}$  electron capture rates and compare them to the values presented by Takahara *et al* [25]. The figure shows also the four transitions

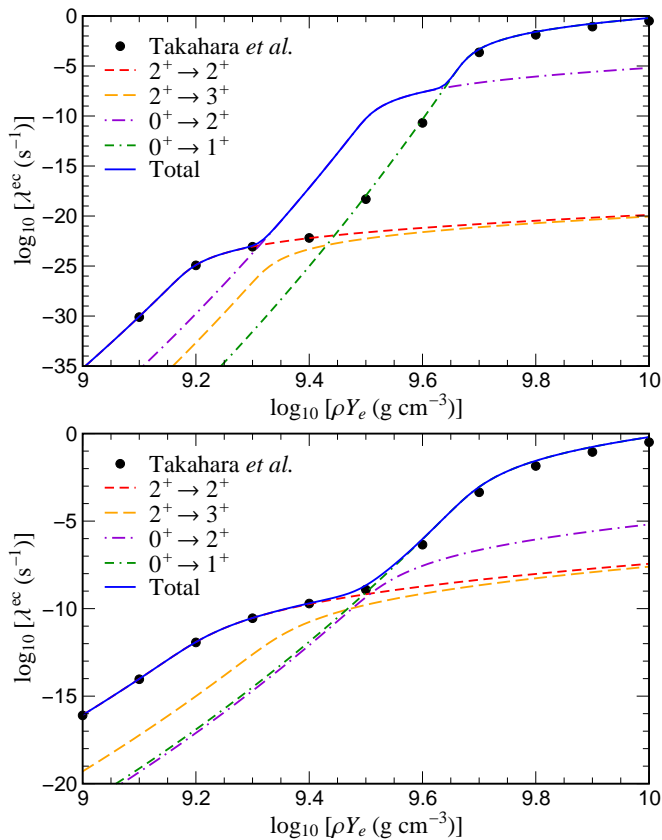


FIG. 1. Comparison of our electron capture rate on  $^{20}\text{Ne}$  as function of density and for selected temperatures (upper panel:  $\log T(\text{K}) = 8.6$ , lower panel:  $\log T(\text{K}) = 9.0$ ) with the values given by Takahara *et al.* [25]. The figure shows the four transitions that fully determine the rate. The rates have not been corrected for medium effects.

that determine the capture rate for the relevant astrophysical conditions. The difference between the contribution of these four transitions and the total rate is less than 1% for the relevant range of temperatures and densities. The values of the  $GT$  matrix elements used are shown in table I.

For densities at which the electron chemical potential is smaller than the electron capture threshold the electron capture rate can be approximated by equation (18), with  $Q = -7.535$  MeV [47]. Transitions to the final ground state are favored, i.e.  $E_f = 0$ , which applies for the allowed transition from the first excited state in  $^{20}\text{Ne}$  and for the non-unique second forbidden ground-state to ground-state transition. Due to the larger transition matrix element for the allowed transition and the lower threshold for capture on the excited state, the allowed transition from the excited  $2^+$  state dominates the rate as low densities, as can be seen in Fig. 1.

With increasing density the electron chemical potential becomes larger and the individual electron capture rates initially increase exponentially (see discussion following Eq. (18)). However, once the electron chemical potential becomes of the order of the threshold for cap-

ture on the  $2^+$  excited state of  $^{20}\text{Ne}$  ( $E_{\text{thres}} = 5.9$  MeV corresponding to  $\log \rho Y_e (\text{g cm}^{-3}) = 9.2$ ), the contribution to the  $^{20}\text{Ne}$  electron capture of the  $2^+$  state behaves according to equation (19); i.e. the rate from the  $2^+$  grows like a power of the electron chemical potential and it is suppressed by the Boltzmann factor  $\exp(-E_i/(kT))$ , with  $E_i = 1.634$  MeV. As the chemical potential is still lower than the threshold for capture on the ground state to either the ground state ( $E_{\text{thres}} = 7.535$  MeV) or to the first  $1^+$  state ( $E_{\text{thres}} = 8.592$  MeV) in  $^{20}\text{F}$  the contributions of these states to the capture rate grow exponentially and indeed dominate the rate at higher densities (see Fig. 1). As the threshold for the non-unique second forbidden transition to the ground state is lower than the one for the allowed transition to the  $1^+$ , it can dominate the rate provided that:

$$\frac{\Lambda^{\text{ec}}(0^+ \rightarrow 2^+)}{\Lambda^{\text{ec}}(0^+ \rightarrow 1^+)} = 0.77 \frac{B(0^+ \rightarrow 2^+)}{B(0^+ \rightarrow 1^+)} \exp\left(\frac{1.057 \text{ MeV}}{kT}\right) > 1. \quad (53)$$

Using the values of the matrix elements from table I, the forbidden contribution dominates the rate for temperatures smaller than 0.9 GK. Figure 1 shows that this is in fact the case, exemplified for the temperature  $\log T(\text{K}) = 8.6$ , in the density range  $\log \rho Y_e (\text{g cm}^{-3}) = 9.3\text{--}9.6$ .

The above results have been obtained assuming an allowed shape for the phase space of the second forbidden transition. The shape factor for non-unique second forbidden transitions can contain additional powers of the electron energy ranging from zero to four [48]. A dependence like  $E_e^2$  will increase the second forbidden rate by a factor 4, while a dependence like  $E_e^4$  will result in a rate a factor 10 larger, compensating the possible overestimate of the matrix element by the current experimental upper limit.

As the second-forbidden transition has not been included in previous rate estimates [5, 25], our rate is larger in the density regime  $\rho Y_e = 2\text{--}4 \times 10^9 \text{ g cm}^{-3}$ . We note that this difference can amount to several orders of magnitude at temperatures below 0.9 GK. Hence even if the forbidden transition strength is somewhat smaller than the current experimental upper limit, this state is likely to dominate the rate in an important temperature-density range for the evolution of the cores of 8–12  $M_{\odot}$  stars.

At densities beyond  $\log \rho Y_e (\text{g cm}^{-3}) = 9.6$ , the rate is given by the  $GT_+$  transition from the  $^{20}\text{Ne}$  ground state to the lowest  $1^+$  state in  $^{20}\text{F}$ . For this transition we use the experimental value determined from the  $(p, n)$  charge-exchange experiment of Ref. [44]. This value is in agreement with the transition strength recently derived from a  $(p, p')$  experiment [49]. In principle the  $GT$  strength can also be obtained from the experimental M1 strength between the respective states. This is, however, model dependent as this M1 transition has a very strong orbital contribution due to the large deformation of  $^{20}\text{Ne}$ . Takahara *et al.* [25] and Oda *et al.* [5] had no access to

the experimental data and used a shell model transition strength instead which, however, was a factor 2 smaller than the experimental value. This explains the difference between our capture rate at high densities to the previous calculations.

The most important conclusion from Fig. 1 is that the electron capture rate on  $^{20}\text{Ne}$  is basically fixed by experimental input, with the exception of the density regime  $\log \rho Y_e (\text{g cm}^{-3}) = 9.3\text{--}9.6$  at temperatures  $T < 10^9$  K, where the forbidden ground-state-to-ground-state transition is likely to determine the rate. To put the rate entirely on experimental values, a measurement of this forbidden transition is highly desirable.

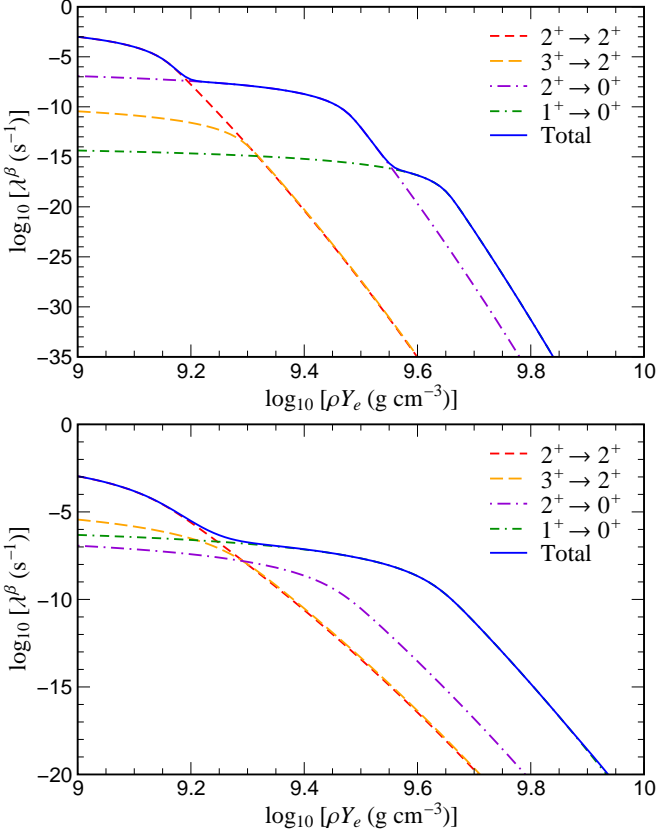


FIG. 2. Beta decay rate of  $^{20}\text{F}$  as a function of density and for selected temperatures (upper panel:  $\log T(\text{K}) = 8.6$ , lower panel:  $\log T(\text{K}) = 9.0$ ). The figure shows the four transitions that fully determine the rate. The rates have not been corrected for medium effects.

The beta-decay rate of  $^{20}\text{F}$  (see Fig. 2) is determined by the same transitions as the electron capture rate on  $^{20}\text{Ne}$ . At low densities the decay is dominated by the transition from the ground state of  $^{20}\text{F}$  to the  $2^+$  excited state of  $^{20}\text{Ne}$ . However, due to the presence of a degenerate electron gas in the stellar environment the beta-decay phase space is reduced which increases the decay half-life with respect to conditions in the laboratory. With increasing density the electron final state blocking becomes more important and for densi-

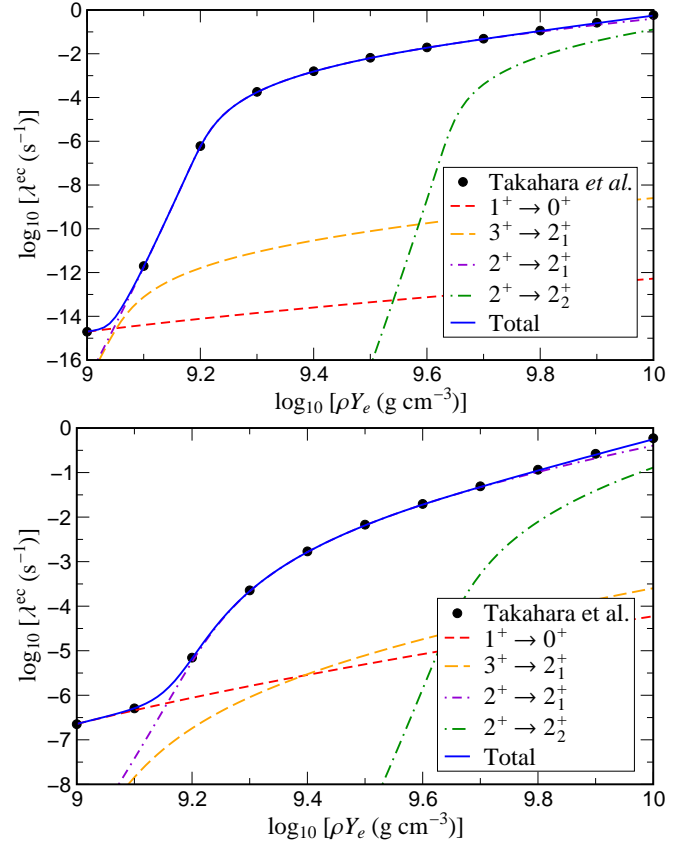


FIG. 3. Comparison of our electron capture rate on  $^{20}\text{F}$  as function of density and for selected temperatures (upper panel:  $\log T(\text{K}) = 8.6$ , lower panel:  $\log T(\text{K}) = 9.0$ ) with the values given by Takahara *et al.* [25]. The rates have not been corrected for medium effects.

ties around  $\log \rho Y_e (\text{g cm}^{-3}) = 9.2$  the above transition is fully blocked. At this moment the decay proceeds primarily by either the ground-state to ground-state second forbidden transition or by the transition from the first  $1^+$  excited state in  $^{20}\text{Ne}$ . The latter transition has a larger phase space but it is suppressed at low temperatures by the Boltzmann factor. Similar to electron capture on  $^{20}\text{Ne}$  the forbidden transition dominates the beta-decay rate for temperatures  $T < 10^9$  K in a density regime above  $\log \rho Y_e (\text{g cm}^{-3}) = 9.2$ .

In Fig. 3 the electron capture rate on  $^{20}\text{F}$  is compared with the values computed by Takahara *et al.* [25]. In the relevant temperature and density range the rate is mainly dominated by the transition from the ground state to the  $2^+$  excited state in  $^{20}\text{O}$ . The matrix elements for the transitions determining the rate are given in table II. The theoretical values have been determined by a shell-model calculation using the USDB interaction [46]. At low densities the rate is determined by the transition from the  $1^+$  excited state of  $^{20}\text{F}$  to the ground state of  $^{20}\text{O}$  which is known experimentally from the beta decay of  $^{20}\text{O}$  [50]. Our electron capture rates on  $^{20}\text{F}$  agree with the previous results [5, 25].

TABLE II. Matrix elements that determine the electron capture rate on  $^{20}\text{F}$  for the relevant temperatures and densities. The ground-state to ground-state electron  $Q$ -value is  $Q_{\text{ec}} = -4.325$  MeV [47].

| Initial $^{20}\text{F}$ state |              | Final $^{20}\text{O}$ state |              | Matrix element      |
|-------------------------------|--------------|-----------------------------|--------------|---------------------|
| $J^\pi$                       | Energy (MeV) | $J^\pi$                     | Energy (MeV) | $B$                 |
| $2^+$                         | 0            | $2_1^+$                     | 1.674        | 0.0229 <sup>a</sup> |
| $2^+$                         | 0            | $2_2^+$                     | 4.072        | 0.0436 <sup>a</sup> |
| $3^+$                         | 0.656        | $2_1^+$                     | 1.674        | 0.0150 <sup>a</sup> |
| $1^+$                         | 1.057        | $0^+$                       | 0            | 0.378 <sup>b</sup>  |

<sup>a</sup> Theoretical value

<sup>b</sup> From  $^{20}\text{O}$  decay [50]

$$\lambda^{\text{ec}}(^{20}\text{Ne}) = \frac{\ln 2}{K} [5e^{-E(2^+)/kT} B_e(2^+ \rightarrow 2^+) \Phi_e^{\text{ec}}(Q(2^+ \rightarrow 2^+), T, \mu_e) + 5e^{-E(2^+)/kT} B_e(2^+ \rightarrow 3^+) \Phi_e^{\text{ec}}(Q(2^+ \rightarrow 3^+), T, \mu_e) + B_e(0^+ \rightarrow 2^+) \Phi_e^{\text{ec}}(Q(0^+ \rightarrow 2^+), T, \mu_e) + B_e(0^+ \rightarrow 1^+) \Phi_e^{\text{ec}}(Q(0^+ \rightarrow 1^+), T, \mu_e)] \quad (54)$$

TABLE III. Numerical values of the quantities that determine the analytical expression for the electron capture rate on  $^{20}\text{Ne}$ .

| Transition   | $Q$ -value | Effective matrix element |
|--|------------|--------------------------|
| $J^\pi(^{20}\text{Ne}) \rightarrow J^\pi(^{20}\text{F})$ | (MeV)      | $B_e$                    |
| $2^+ \rightarrow 2^+$                                    | -5.902     | 0.0835                   |
| $2^+ \rightarrow 3^+$                                    | -6.558     | 0.0827                   |
| $0^+ \rightarrow 2^+$                                    | -7.536     | $1.23 \times 10^{-6}$    |
| $0^+ \rightarrow 1^+$                                    | -8.592     | 0.324                    |

The function  $\Phi_e^{\text{ec}}$  is defined in equation (15). All other quantities necessary for the evaluation of the rate are defined in table III. The difference between the effective transition matrix element,  $B_e$ , appearing in table III

The rates shown in figures 1, 2 and 3 show clear kinks that mark the transition between density regimes which are dominated by different individual transitions. Obviously the kinks get smeared out with increasing temperature. In astrophysical simulations a reliable resolution of the kinks requires either a very fine grid for the tabulation of the rates or an analytical expression. We will provide this analytical expression in the following.

For electron capture on  $^{20}\text{Ne}$  we can write the electron capture rate, based on the 4 transitions identified above, as:

and the matrix element,  $B$ , of table I is due to the fact that the former includes the average value of the Fermi Coulomb distortion function. This value is equal to 1.267 for  $Z = 10$ . Equation (54) reproduces the electron capture rate on  $^{20}\text{Ne}$  if one uses “exact” numerical values for the Fermi integrals. Using the approximate expressions of the Fermi function defined in eq. (16), the largest error is around 15%. This uncertainty occurs when the electron fermi energy is of the order of the  $Q$ -value of the dominating transition. The origin of the uncertainty is mainly due to the approximation made in the Fermi integral of order 2 in equation (16c).

The beta-decay rate of  $^{20}\text{F}$  is given by the same 4 transitions as the electron capture on  $^{20}\text{Ne}$  for the astrophysically relevant conditions of interest here. The rate can then be written as:

$$\lambda^\beta(^{20}\text{F}) = \frac{\ln 2}{5K} [5B_e(2^+ \rightarrow 2^+) \Phi_e^\beta(Q(2^+ \rightarrow 2^+), T, \mu_e) + 7e^{-E(3^+)/kT} B_e(3^+ \rightarrow 2^+) \Phi_e^\beta(Q(3^+ \rightarrow 2^+), T, \mu_e) + 5B_e(2^+ \rightarrow 0^+) \Phi_e^\beta(Q(2^+ \rightarrow 0^+), T, \mu_e) + 3e^{-E(1^+)/kT} B_e(1^+ \rightarrow 0^+) \Phi_e^\beta(Q(1^+ \rightarrow 0^+), T, \mu_e)] \quad (55)$$

The function  $\Phi_e^\beta$  is defined in equation (31). All other quantities necessary for the evaluation of the rate are defined in table IV. Similarly to the case of electron capture on  $^{20}\text{Ne}$  the rate is reproduced “exactly” if the Fermi integrals are evaluated to numerical precision and errors

of around 15% are obtained if one uses the approximate expressions defined in eq. (16).

Finally, the electron capture rate on  $^{20}\text{F}$  can be written as:

TABLE IV. Numerical values of the quantities that determine the analytical expression for the beta decay rate of  $^{20}\text{F}$ .

| Transition<br>$J^\pi(^{20}\text{F}) \rightarrow J^\pi(^{20}\text{Ne})$ | $Q$ -value<br>(MeV) | Effective matrix element<br>$B_e$ |
|--|---------------------|-----------------------------------|
| $2^+ \rightarrow 2^+$  | 5.902               | 0.0835                            |
| $3^+ \rightarrow 2^+$  | 6.558               | 0.0591                            |
| $2^+ \rightarrow 0^+$  | 7.536               | $2.46 \times 10^{-7}$             |
| $1^+ \rightarrow 0^+$  | 8.592               | 0.108                             |

$$\lambda^{\text{ec}}(^{20}\text{F}) = \frac{\ln 2}{5K} [3e^{-E(1^+)/kT} B_e(1^+ \rightarrow 0^+) \Phi_e^{\text{ec}}(Q(1^+ \rightarrow 0^+), T, \mu_e) + 7e^{-E(3^+)/kT} B_e(3^+ \rightarrow 2_1^+) \Phi_e^{\text{ec}}(Q(3^+ \rightarrow 2_1^+), T, \mu_e) + 5B_e(2^+ \rightarrow 2_1^+) \Phi_e^{\text{ec}}(Q(2^+ \rightarrow 2_1^+), T, \mu_e) + 5B_e(2^+ \rightarrow 2_2^+) \Phi_e^{\text{ec}}(Q(2^+ \rightarrow 2_2^+), T, \mu_e)] \quad (56)$$

TABLE V. Numerical values of the quantities that determine the analytical expression for the electron capture on  $^{20}\text{F}$ .

| Transition<br>$J^\pi(^{20}\text{F}) \rightarrow J^\pi(^{20}\text{Ne})$ | $Q$ -value<br>(MeV) | Effective matrix element<br>$B_e$ |
|--|---------------------|-----------------------------------|
| $1^+ \rightarrow 0^+$  | -3.268              | 0.467                             |
| $3^+ \rightarrow 2_1^+$  | -5.342              | 0.0185                            |
| $2^+ \rightarrow 2_1^+$  | -5.998              | 0.0283                            |
| $2^+ \rightarrow 2_2^+$  | -8.397              | 0.0539                            |

The quantities necessary for the evaluation of the rate are defined in table V. The difference between the effective transition matrix element,  $B_e$ , appearing in table V and the matrix element,  $B$ , of table II is due to the fact that the former includes the average value of the Fermi Coulomb distortion function. This value is equal to 1.236 for  $Z = 9$ .

The above expressions can be generalized to the calculation of the neutrino energy loss rate by simply substituting the function  $\Phi$  by  $\Psi$  defined in equations (22) and (37) for electron capture and beta-decay, respectively.

Coulomb corrections are an important modification of weak interaction rates in dense astrophysical environment. In the following we include screening corrections in our rates following the generalization of the screening treatment, as originally developed by Bravo and Garcia-Senz [51], and presented in detail for electron capture in the appendix of Ref. [14]. Screening has two effects on electron capture: the threshold energy in the medium is increased,  $Q_{if}^{\text{ec,med}} = Q_{if}^{\text{ec}} - \Delta Q_c(Z)$  (notice that  $Q_{if}$  is negative in our convention), and the chemical potential of the electrons is reduced,  $\mu_e^{\text{med}} = \mu_e - V_s$ , where the parameters  $\Delta Q_c(Z)$  and  $V_s$  can be calculated following [14, 51, 52]. We note that both effects reduce the electron capture rate. The opposite is true for  $\beta^-$  decays where screening enhances the rate. At first, the lowering of the electron chemical potential re-

sults in reduction of the Pauli blocking in the final state, i.e. smaller values of  $(1 - S_e(\omega))$  in Eq. (3b). Secondly, for beta decays the change in threshold is given by  $Q_{if}^{\beta,\text{med}} = Q_{if}^\beta + \Delta Q_c(Z + 1)$  (note that  $Q_{if}^\beta = -Q_{if}^{\text{ec}}$ ).

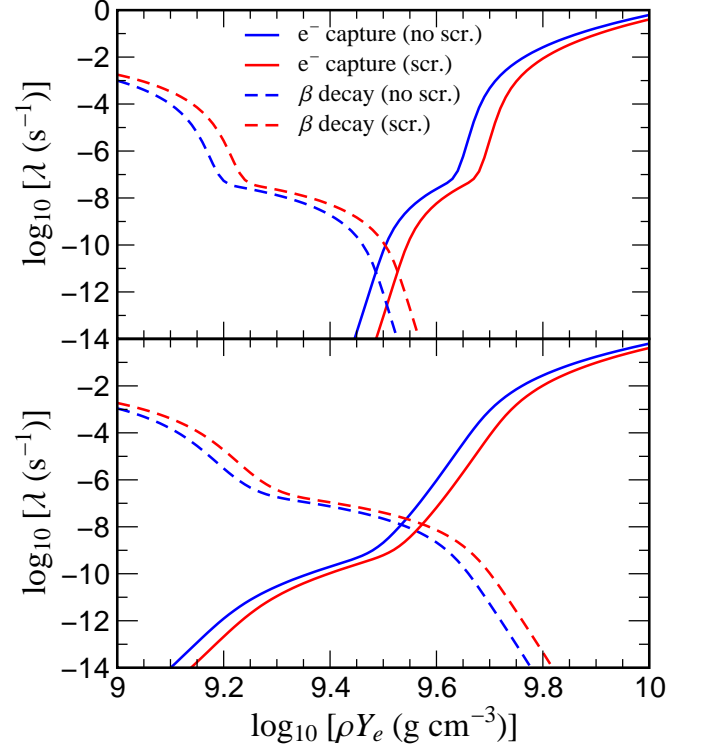


FIG. 4. Electron capture rate on  $^{20}\text{Ne}$  and beta decay rate of  $^{20}\text{F}$  with and without consideration of medium corrections (upper panel:  $\log T(\text{K}) = 8.6$ , lower panel:  $\log T(\text{K}) = 9.0$ ).

To demonstrate the effect of screening we show in figure 4 the electron capture rate on  $^{20}\text{Ne}$  and the beta decay rate of  $^{20}\text{F}$  with and without consideration of Coulomb corrections. Obviously the effect is largest at

low temperatures as both rates are more sensitive to modifications of the threshold energy which changes by 120 keV at the lowest and by 270 keV at the highest density considered in Fig. 4. More importantly, screening corrections change the density at which electron capture dominates over beta-decay and can potentially affect the evolution of the star [53]. In particular the Coulomb modifications shift the densities at which URCA pairs operate in stars to higher densities.

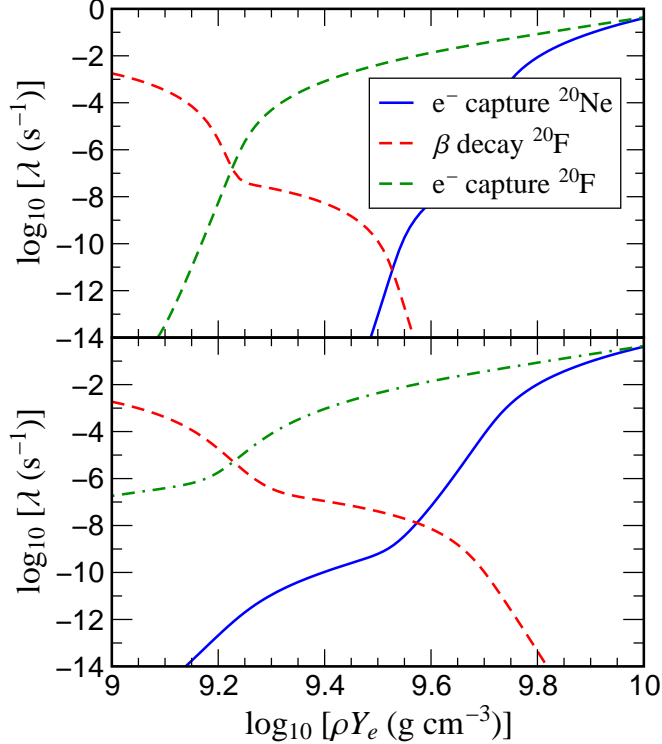


FIG. 5. Rates for electron captures on  $^{20}\text{Ne}$  and  $^{20}\text{F}$  and beta-decay of  $^{20}\text{F}$  for selected temperatures:  $\log T(\text{K}) = 8.6$  (upper panel),  $\log T(\text{K}) = 9.0$  (lower panel). Medium corrections are included in the rates.

In Fig. 5 we compare the  $^{20}\text{Ne}$  electron capture rate with the rates for the competing  $^{20}\text{F}$   $\beta$  decay and electron capture, considering Coulomb corrections as discussed above. We observe that the electron capture rate gets larger than the competing  $^{20}\text{F}$  decay rate for densities larger than  $\rho Y_e \approx 4 \times 10^9 \text{ g cm}^{-3}$ . As the electron capture rate on  $^{20}\text{F}$  is faster than the one on  $^{20}\text{Ne}$ , caused by the smaller  $Q$ -value, the capture on  $^{20}\text{Ne}$  is followed by a second capture process leading to  $^{20}\text{O}$ .

At the densities of concern here the neutrinos produced in the electron captures and  $\beta$  decays leave the star unhindered and carry away energy. Depending on the amount of energy carried away, weak processes can result in a net heating or cooling of the stellar environment. This depends on the sign of the quantity  $\mathcal{E}$  defined in equations (50a) and (50b). Figure 6 shows  $\mathcal{E}$ , i.e. the average energy produced or absorbed by the various processes (electron capture on  $^{20}\text{Ne}$ , beta-decay of  $^{20}\text{F}$

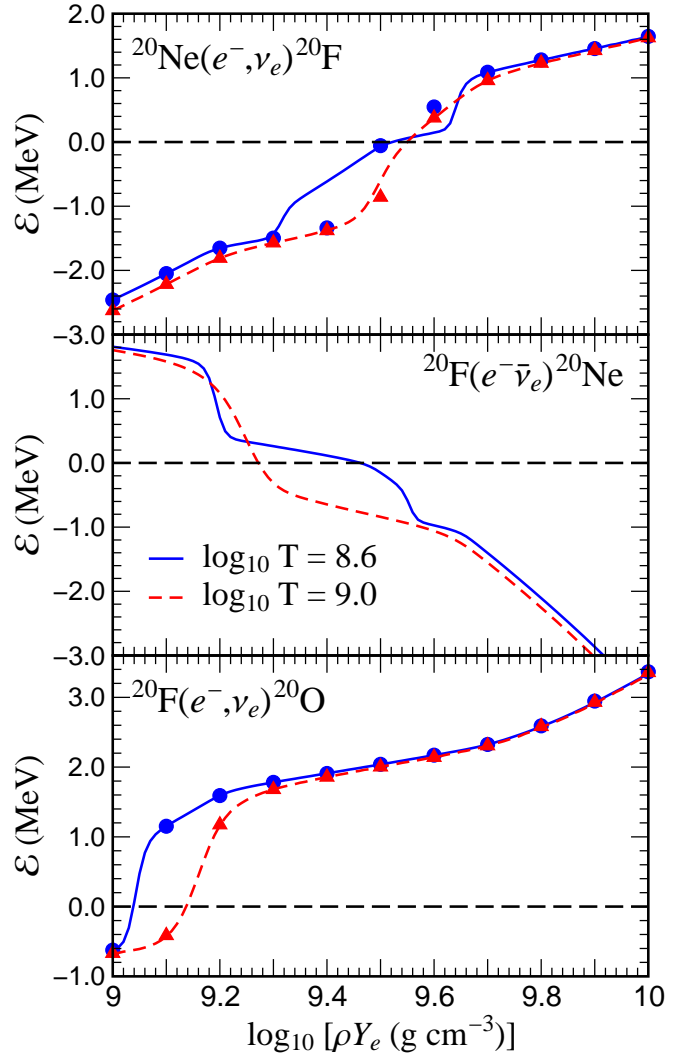


FIG. 6. Average energy produced (positive) or absorbed (negative) by electron capture on  $^{20}\text{Ne}$  (upper panel), beta-decay of  $^{20}\text{F}$  (middle panel) and electron capture on  $^{20}\text{F}$  (lower panel).

and electron capture on  $^{20}\text{F}$ ) compared with the values provided by Takahara *et al.* [25]. As discussed in section II C at low densities, electron capture is endothermic as energy has to be absorbed from the medium to populate the excited states that dominate the rate. Under these conditions the average energy grows proportional to  $\mu_e \approx \rho^{1/3}$  until the rate is dominated by a different transition. At this moment a sudden change in the growth of the energy generation takes place. For  $^{20}\text{Ne}$  this transition occurs for densities  $\log \rho Y_e (\text{g cm}^{-3}) \approx 9.3$  and temperatures smaller than 1 GK, when the rate is dominated by the second-forbidden transition to the  $^{20}\text{F}$  ground state for both the electron capture on  $^{20}\text{Ne}$  and the beta-decay of  $^{20}\text{F}$ . As this transition was not included in the work of Takahara *et al* [25], we predict substantially different values for the energy generation. In the case of beta-decay, whenever the energy genera-

tion is dominated by a particular transition it decreases like  $\mu_e/4$  (see section II C) and it is positive up to densities for which  $\mu_e$  equals the ground-state to ground-state  $Q$ -value. At these densities, the  $^{20}\text{Ne}$  electron capture rate energy generation becomes positive and changes its growth behavior to  $\mu_e/4$  while beta-decay, being Pauli blocked, decreases like  $-\mu_e$ . Due to the smaller  $Q$ -value for electron capture on  $^{20}\text{F}$  the average energy produced is positive for most of the density region shown in figure 6. For densities larger than  $\log \rho Y_e (\text{g cm}^{-3}) \approx 9.2$  the energy produced by electron capture on  $^{20}\text{F}$  dominates over the energy loss by capture on  $^{20}\text{Ne}$  and makes the net energy generation positive. This density marks the transition at which the net effect of the sequence of weak-interaction processes changes from endothermic to exothermic and, correspondingly, the core temperature increases in stellar evolution models [24]. The increase in the energy generation by electron capture on  $^{20}\text{F}$  at high densities is due to the contribution of transitions to excited states on  $^{20}\text{O}$  (see figure 3) that increase the average gamma energy in equation (52). We note that the transition at which electron capture on  $^{20}\text{Ne}$  becomes exothermic occurs at slightly higher densities than for the capture on  $^{20}\text{F}$ . This is due to pairing effects which makes the  $Q$  value for the transition from an even-even nucleus to an odd-odd nucleus larger than the neighboring one from an odd-odd to an even-even nucleus.

### B. Rates for the $A = 24$ nuclei

Since the evaluation of the electron capture rate on  $^{24}\text{Mg}$  by Takahara *et al.* [25] and by Oda *et al.* [5], several important experimental data sets became available. These include an improved measurement of the  $\beta$  decay of the  $1^+$  isomeric state in  $^{24}\text{Al}$  which, assuming isospin symmetry, determines the GT transition from the analogue state in  $^{24}\text{Na}$  at  $E_x = 0.426$  MeV to the  $^{24}\text{Mg}$  ground state and the two excited  $2^+$  states at  $E_x = 1.369$  MeV and 4.238 MeV [54]. The GT strength has also been measured by  $(p, n)$  [44],  $(^3\text{He}, t)$  [55],  $(t, ^3\text{He})$  [56] and  $(d, ^2\text{He})$  [57] charge-exchange reactions where the first two can be applied in the case of  $^{24}\text{Mg}$  due to the isospin symmetry of the nucleus. The various measurements basically agree on the  $B(GT)$  value for the transition from the  $1^+$  isomeric state to the ground state which, as we will see below, determines the electron capture rate on  $^{24}\text{Mg}$  for a large range of the astrophysically relevant temperatures and densities. In the following we will adopt the value  $B(GT) = 0.094(3)$ , derived from the  $\beta^+$  decay, for this transition. It is slightly larger than the values determined from the charge-exchange experiments ( $B(GT) = 0.079(2)$  from  $(p, n)$  [44],  $B(GT) = 0.086(2)$  from  $(^3\text{He}, t)$  [55],  $0.078(8) \pm 0.04$  from  $(d, ^2\text{He})$  [57]), except the strength determined by  $(t, ^3\text{He})$  [56],  $B(GT) = 0.13(2)$  that cannot be separated from the nearby  $2^+$  state. However, the value adopted by us is noticeably larger than the  $B(GT)$  value used in the

previous electron capture rate evaluations [5, 25] derived from  $\beta$  decay data available at the time these works were performed.

In details, our input for the calculation of the  $^{24}\text{Mg}$  electron capture rate is based on the  $^{24}\text{Al}$   $\beta^+$  decay data supplying the  $GT$  transitions from the ground state and the lowest two  $2^+$  states in  $^{24}\text{Mg}$  to the  $1^+$  state in  $^{24}\text{Na}$  at  $E_x = 472$  keV. From the  $^{24}\text{Na}$   $\beta^-$  decay of the  $4^+$  ground state we adopt the  $GT$  transitions from the first  $4^+$  state in  $^{24}\text{Mg}$  at  $E_x = 4.123$  MeV and the second-forbidden transition from the  $2^+$  state at  $E_x = 1.369$  MeV. The GT values from the ground state to the other excited  $1^+$  states are taken from the  $(^3\text{He}, t)$  experiment of Ref. [55]. Finally, we supplement these data by GT strength distributions for excited states in  $^{24}\text{Mg}$  derived from shell model calculations performed in the sd shell and using the USDB interaction. We note that, due to the strong angular momentum mismatch, forbidden transitions to the  $^{24}\text{Na}$   $4^+$  ground state do not contribute to the capture rate. The energies and  $B(GT)$  values which determine the  $^{24}\text{Mg}$  electron capture and  $\beta$ -decay rates at the conditions of interest here are summarized in Table VI.

TABLE VI. Information that determines the electron capture rate on  $^{24}\text{Mg}$  and beta decay of  $^{24}\text{Na}$  for the relevant temperatures and densities. The ground-state to ground-state electron  $Q$ -value is  $Q_{\text{ec}} = -6.026$  MeV [47].

| Initial $^{24}\text{Mg}$ state |              | Final $^{24}\text{Na}$ state |              | Matrix element                       |
|--------------------------------|--------------|------------------------------|--------------|--------------------------------------|
| $J^\pi$                        | Energy (MeV) | $J^\pi$                      | Energy (MeV) | $B$                                  |
| $0^+$                          | 0            | $1^+$                        | 0.472        | 0.094(3) <sup>a</sup>                |
| $0^+$                          | 0            | $1_2^+$                      | 1.347        | 1.038(87) <sup>b</sup>               |
| $0^+$                          | 0            | $1_3^+$                      | 1.89         | 0.040(13) <sup>b</sup>               |
| $0^+$                          | 0            | $1_4^+$                      | 3.41         | 0.460(38) <sup>b</sup>               |
| $2^+$                          | 1.369        | $4^+$                        | 0.0          | $5.0(3) \times 10^{-8}$ <sup>c</sup> |
| $2^+$                          | 1.369        | $1^+$                        | 0.472        | 0.0046(11) <sup>a</sup>              |
| $2^+$                          | 1.369        | $2^+$                        | 0.563        | 0.032 <sup>d</sup>                   |

<sup>a</sup> From decay of mirror  $^{24}\text{Al}$  [54]

<sup>b</sup> From  $(d, ^2\text{He})$  [57]

<sup>c</sup> From  $^{24}\text{Na}$  decay [58]

<sup>d</sup> Theoretical value

Fig. 7 shows the electron capture rate on  $^{24}\text{Mg}$  in the astrophysically relevant density range and for selected temperatures, not considering medium-induced Coulomb corrections. For densities  $9.0 < \log \rho Y_e (\text{g cm}^{-3}) < 9.5$  and the relevant temperature regime ( $T = 0.4 - 1.0$ ) GK the rate is dominated by the capture from the  $^{24}\text{Mg}$  ground state to the isomeric state in  $^{24}\text{Na}$  at  $E_x = 0.472$  MeV. At the highest temperatures (the lower panel of Fig. 7 shows the rate for  $T = 10^9$  K) the excited state at  $E_x = 1.369$  MeV gets sufficiently thermally populated that its transitions to the excited  $1^+$  state at  $E_x = 0.472$  MeV and  $2^+$  state at  $E_x = 0.563$  MeV slightly contribute to the rate at densities  $\log \rho Y_e (\text{g cm}^{-3}) < 9.1$ . At higher densities  $\log \rho Y_e (\text{g cm}^{-3}) > 9.5$  the most im-

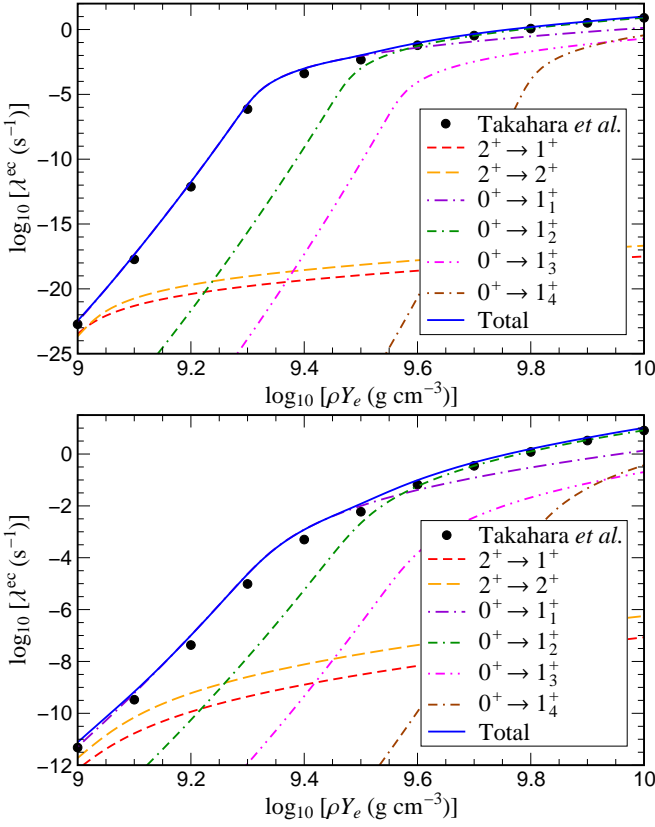


FIG. 7. Comparison of our electron capture rate on  $^{24}\text{Mg}$  as function of density and for selected temperatures (upper panel:  $\log T(\text{K}) = 8.6$ , lower panel:  $\log T(\text{K}) = 9.0$ ) with the values given by Takahara *et al.* [25]. The figure shows the six transitions that fully determine the rate. The rates have not been corrected for medium effects.

portant contribution to the rate comes from the strong GT transition from the ground state to the  $1^+$  state at  $E_x = 1.347$  MeV ( $B(\text{GT}) = 1.038(87)$  [57]) which is more than 10 times larger than the one to the state at  $E_x = 0.472$  MeV and compensates for the larger phase space factor of the latter at the higher densities. Due to its large  $B(\text{GT})$  value of 0.46, the transition from the ground state to the  $1^+$  state at  $E_x = 3.41$  MeV contributes on the few percent level at  $\log \rho Y_e (\text{g cm}^{-3}) = 10$ . The electron capture rate on  $^{24}\text{Mg}$  presented here is entirely based on experimental input, except for the small contributions arising from the ground state transitions to the lowest excited  $1^+$  and  $2^+$  states, for which we adopt the  $B(\text{GT})$  values from a shell model calculation. These transitions, however, modify the rate only at low densities ( $\log \rho Y_e (\text{g cm}^{-3}) < 9.1$ ) and the highest temperatures of interest.

The present rate is somewhat larger than the one given by Takahara *et al.* [25] and by Oda *et al.* [5]. The main difference comes from the increase in the  $B(\text{GT})$  value for the ground state transition to the  $1^+$  state at 472 keV where recent experiments [54, 55] indicate a noticeably larger value than deduced from  $^{24}\text{Al}$  decay data available

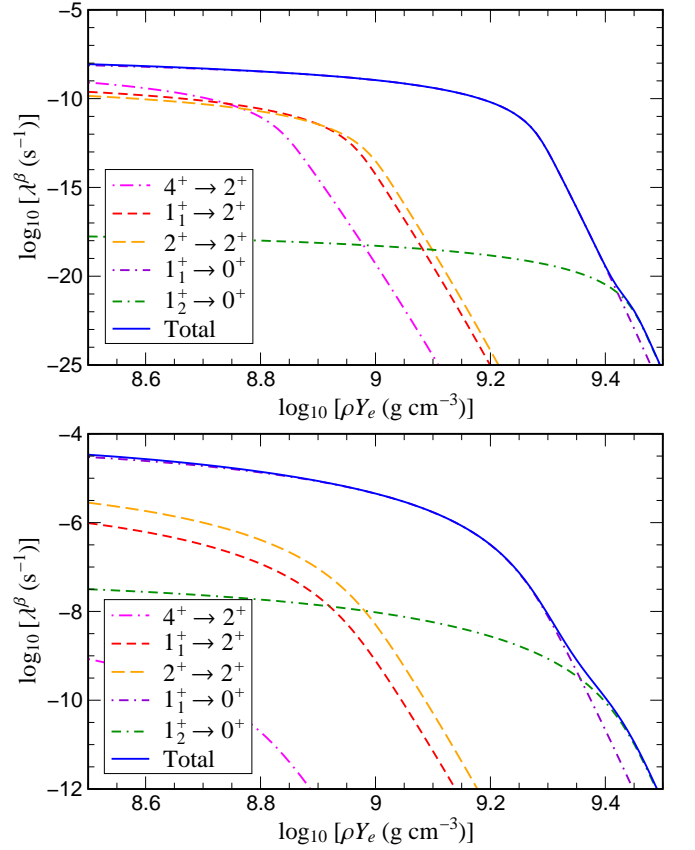


FIG. 8. Beta decay of  $^{24}\text{Na}$  as a function of density and for selected temperatures (upper panel:  $\log T(\text{K}) = 8.6$ , lower panel:  $\log T(\text{K}) = 9.0$ ). The figure shows the five transitions that fully determine the rate. The rates have not been corrected for medium effects.

at the time of the Takahara *et al.* [25] and Oda *et al.* [5] works.

Electron capture on  $^{24}\text{Mg}$  stands in competition with the  $\beta$  decay of the daughter  $^{24}\text{Na}$ . We have evaluated this  $\beta$ -decay rate on the basis of the same transitions as adopted in our calculation of the  $^{24}\text{Mg}$  electron capture and summarized in Table VI. For the conditions of interest here we find that the  $^{24}\text{Na}$   $\beta$  decay is mainly given by the GT transition from the isomeric  $1^+$  state at excitation energy  $E_x = 472$  keV to the  $^{24}\text{Mg}$  ground state, where the GT strength is known from the decay of the mirror state in  $^{24}\text{Al}$ . However, this contribution depends strongly on temperature via the thermal population of the initial state. Hence with decreasing temperature the second-forbidden transition from the  $^{24}\text{Na}$   $4^+$  ground state to the  $2^+$  state in  $^{24}\text{Mg}$  at  $E_x = 1.369$  MeV grows in importance. This transition strength is known experimentally from the  $\beta$  decay of  $^{24}\text{Na}$  [58]. We note that at low temperatures (the upper panel of Fig. 8 shows the  $\beta$  decay rate at  $T = 0.4$  GK) and low densities ( $\log \rho Y_e (\text{g cm}^{-3}) < 8.75$ ) this forbidden transition contributes already of order 10% to the total decay rate, and becomes relatively more important at even smaller

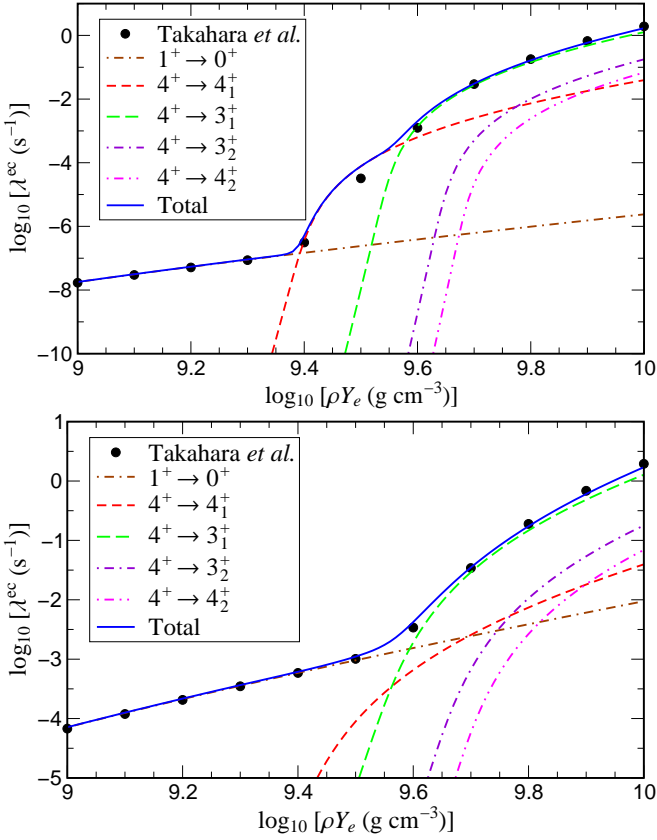


FIG. 9. Comparison of our electron capture rate on  $^{24}\text{Na}$  as function of density and for selected temperatures (upper panel:  $\log T(\text{K}) = 8.6$ , lower panel:  $\log T(\text{K}) = 9.0$ ) with the values given by Takahara *et al.* [25]. The figure shows the five transitions that determine the rate. The rates have not been corrected for medium effects.

temperatures. The contribution of this transition has been determined assuming an allowed shape for the phase space. As discussed for  $^{20}\text{Ne}$ , it can become even larger if the phase space deviates from the allowed shape. The GT transition from the isomeric  $1^+$  state to the ground state gets Pauli blocked by the presence of the electron sea at densities of order ( $\log(\rho Y_e) \approx 9.3$ ), explaining the strong decrease in its partial rate. Hence at higher densities the transition from the second  $1^+$  excited state at  $E_x = 1.347$  MeV to the ground state, having a larger decay energy, contributes more strongly to the rate, in particular at the higher temperatures. Finally we mention that the GT decay from the  $^{24}\text{Na}$  ground state to the excited state at  $E_x = 4.123$  MeV in  $^{24}\text{Mg}$ , which overwhelmingly dominates the  $^{24}\text{Na}$   $\beta$  decay under terrestrial conditions is strongly Pauli-blocked under astrophysical conditions with densities  $\rho Y_e > 10^8 \text{ g cm}^{-3}$ .

In Fig. 9 we have plotted the electron capture rate on  $^{24}\text{Na}$  at two selected temperatures and the densities of

relevance for the evolution of the ONeMg core in 8–12  $M_\odot$  stars. We have evaluated the rate based on experimental energies and shell model GT transition rates, supple-

TABLE VII. Information that determines the electron capture rate on  $^{24}\text{Na}$ . The ground-state to ground-state electron  $Q$ -value is  $Q_{\text{ec}} = -2.977$  MeV [47].

| Initial $^{24}\text{Na}$ state |              | Final $^{24}\text{Ne}$ state |                    | Matrix element               |
|--------------------------------|--------------|------------------------------|--------------------|------------------------------|
| $J^\pi$                        | Energy (MeV) | $J^\pi$                      | Energy (MeV)       | $B$                          |
| $4^+$                          | 0            | $4^+$                        | 3.972              | $3.8 \times 10^{-3\text{a}}$ |
| $4^+$                          | 0            | $3^+$                        | 4.817 <sup>a</sup> | 0.232 <sup>a</sup>           |
| $4^+$                          | 0            | $3^+$                        | 5.436 <sup>a</sup> | 0.058 <sup>a</sup>           |
| $4^+$                          | 0            | $4^+$                        | 5.691 <sup>a</sup> | 0.030 <sup>a</sup>           |
| $1^+$                          | 0.472        | $0^+$                        | 0.0                | 0.091(2) <sup>b</sup>        |

<sup>a</sup> Theoretical value

<sup>b</sup> From  $^{24}\text{Ne}$  decay [59]

mented by data from the decay of  $^{24}\text{Ne}$  [59]. In particular, we include the GT strengths build on all states till 2.5 MeV excitation energy. The energies and strengths for the transitions that are relevant to determine the rate are summarized in Table VII. We confirm the results discussed in Ref. [25]. At low densities ( $\log(\rho Y_e) < 9.4$ ) the rate is dominated by the GT transition from the thermally populated isomeric  $1^+$  state at  $E_x = 472$  keV to the  $^{24}\text{Ne}$  ground state, while at the largest densities of interest ( $\log(\rho Y_e) \sim 9.6$ –10) the transition from the  $^{24}\text{Na}$   $4^+$  ground state to the first excited  $3^+$  has the largest contribution to the total capture rate, with minor corrections from the GT transition from the ground state to the second excited  $3^+$  state. Our shell model calculations gives quite similar transition strengths than the one performed by [25]. Hence our rates agree quite well with the previous one in the respective density ranges. However, at intermediate densities ( $\log(\rho Y_e) \sim 9.4$ –9.6) the rate is dominated by the transition from the  $^{24}\text{Na}$  ground state to the excited  $4^+$  state in  $^{24}\text{Ne}$ . For this transition our calculation predicts a slightly larger GT value than used in ref. [25],  $B = 1.5 \times 10^{-3}$ , explaining the rate differences in this intermediate regime. (Both, our calculations based on the USDB [46] and the calculations of Takahara *et al.* [25] based on the USD interaction [29] predict a very small matrix element and consequently are rather sensitive to the relatively small differences between the USD and USDB interactions.) As the relevance of this contribution decreases with increasing temperature, our  $^{24}\text{Na}$  electron capture rate becomes similar to the one of Ref. [25] at higher temperatures.

As the electron capture and  $\beta$ -decay rates for the  $A = 24$  nuclei, presented here, are dominated by a few states we can derive analytical rate expressions, following the procedure as outlined above for the  $A = 20$  nuclei. For electron capture on  $^{24}\text{Mg}$  we can write the electron capture rate, based on the 6 transitions identified above, as:

$$\begin{aligned} \lambda^{\text{ec}}(^{24}\text{Mg}) = \frac{\ln 2}{K} & \left[ 5e^{-E(2^+)/kT} B_e(2^+ \rightarrow 1^+) \Phi_e^{\text{ec}}(Q(2^+ \rightarrow 1^+), T, \mu_e) + 5e^{-E(2^+)/kT} B_e(2^+ \rightarrow 2^+) \Phi_e^{\text{ec}}(Q(2^+ \rightarrow 2^+), T, \mu_e) \right. \\ & + B_e(0^+ \rightarrow 1_1^+) \Phi_e^{\text{ec}}(Q(0^+ \rightarrow 1_1^+), T, \mu_e) + B_e(0^+ \rightarrow 1_2^+) \Phi_e^{\text{ec}}(Q(0^+ \rightarrow 1_2^+), T, \mu_e) \\ & \left. + B_e(0^+ \rightarrow 1_3^+) \Phi_e^{\text{ec}}(Q(0^+ \rightarrow 1_3^+), T, \mu_e) + B_e(0^+ \rightarrow 1_4^+) \Phi_e^{\text{ec}}(Q(0^+ \rightarrow 1_4^+), T, \mu_e) \right]. \end{aligned} \quad (57)$$

TABLE VIII. Numerical values of the quantities that determine the analytical expression for the electron capture rate on  $^{24}\text{Mg}$ .

| Transition<br>$J^\pi(^{24}\text{Mg}) \rightarrow J^\pi(^{24}\text{Na})$ | $Q$ -value<br>(MeV) | Effective matrix element<br>$B_e$ |
|---|---------------------|-----------------------------------|
| $2^+ \rightarrow 1^+$   | -5.129              | 0.00613                           |
| $2^+ \rightarrow 2^+$   | -5.220              | 0.0426                            |
| $0^+ \rightarrow 1_1^+$   | -6.498              | 0.125                             |
| $0^+ \rightarrow 1_2^+$   | -7.373              | 1.383                             |
| $0^+ \rightarrow 1_3^+$   | -7.916              | 0.0533                            |
| $0^+ \rightarrow 1_4^+$   | -9.436              | 0.613                             |

The quantities necessary for the evaluation of the rate

$$\begin{aligned} \lambda^\beta(^{24}\text{Na}) = \frac{\ln 2}{9K} & \left[ 9B_e(4^+ \rightarrow 2^+) \Phi_e^\beta(Q(4^+ \rightarrow 2^+), T, \mu_e) + 3e^{-E(1_1^+)/kT} B_e(1_1^+ \rightarrow 2^+) \Phi_e^\beta(Q(1_1^+ \rightarrow 2^+), T, \mu_e) \right. \\ & + 5e^{-E(2^+)/kT} B_e(2^+ \rightarrow 2^+) \Phi_e^\beta(Q(2^+ \rightarrow 2^+), T, \mu_e) + 3e^{-E(1_1^+)/kT} B_e(1_1^+ \rightarrow 0^+) \Phi_e^\beta(Q(1_1^+ \rightarrow 0^+), T, \mu_e) \\ & \left. + 3e^{-E(1_2^+)/kT} B_e(1_2^+ \rightarrow 0^+) \Phi_e^\beta(Q(1_2^+ \rightarrow 0^+), T, \mu_e) \right]. \end{aligned} \quad (58)$$

The quantities necessary for the evaluation of the rate are defined in table IX. Equation (58) reproduces the beta-decay rate of  $^{24}\text{Na}$  with a maximum error of around 20% using the approximate expressions of the Fermi function defined in eq. (16). The maximum error occurs at

are defined in table VIII. The difference between the effective transition matrix element,  $B_e$ , appearing in table VIII and the matrix element,  $B$ , of table VI is due to the fact that the former includes the average value of the Fermi Coulomb distortion function. This value is equal to 1.332 for  $Z = 12$ . Equation (57) reproduces the electron capture rate on  $^{24}\text{Mg}$  with a maximum error of about 20% using the approximate expressions of the Fermi function defined in eq. (16). The maximum error occurs at densities  $\log(\rho Y_e) = 9.3$  where the electron chemical becomes of the order of the electron capture  $Q$ -value, for other conditions the error is of a few percent.

The beta-decay rate of  $^{24}\text{Na}$  is given by the 5 transitions shown in figure 8 for the astrophysical conditions of interest. The rate can then be written as:

densities  $\log(\rho Y_e) = 9.3$  where the electron chemical becomes of the order of the electron capture  $Q$ -value, for other conditions the error is of a few percent.

Finally, the electron capture rate on  $^{24}\text{Na}$  can be written as:

$$\begin{aligned} \lambda^{\text{ec}}(^{24}\text{Na}) = \frac{\ln 2}{9K} & \left[ 3e^{-E(1^+)/kT} B_e(1^+ \rightarrow 0^+) \Phi_e^{\text{ec}}(Q(1^+ \rightarrow 0^+), T, \mu_e) + 9B_e(4^+ \rightarrow 4_1^+) \Phi_e^{\text{ec}}(Q(4^+ \rightarrow 4_1^+), T, \mu_e) \right. \\ & + 9B_e(4^+ \rightarrow 3_1^+) \Phi_e^{\text{ec}}(Q(4^+ \rightarrow 3_1^+), T, \mu_e) + 9B_e(4^+ \rightarrow 3_2^+) \Phi_e^{\text{ec}}(Q(4^+ \rightarrow 3_2^+), T, \mu_e) \\ & \left. + 9B_e(4^+ \rightarrow 4_2^+) \Phi_e^{\text{ec}}(Q(4^+ \rightarrow 4_2^+), T, \mu_e) \right]. \end{aligned} \quad (59)$$

The quantities necessary for the evaluation of the rate are defined in table X. The difference between the effective transition matrix element,  $B_e$ , appearing in table X and the matrix element,  $B$ , of table VII is due to the fact that the former includes the average value of the Fermi Coulomb distortion function. This value is equal to 1.299 for  $Z = 11$ . Equation (59) reproduces the beta-decay rate of  $^{24}\text{Na}$  with a maximum error of around 10% at tem-

peratures around  $\log T(\text{K}) = 8.6$  using the approximate expressions of the Fermi function defined in eq. (16). The maximum error occurs at densities  $\log(\rho Y_e) = 9.4$  where the electron chemical becomes of the order of the electron capture  $Q$ -value for the transition  $4^+ \rightarrow 4_1^+$ . With increasing temperature or for other densities the error is of a few percent.

As explained above medium corrections decrease the

TABLE IX. Numerical values of the quantities that determine the analytical expression for the beta decay rate of  $^{24}\text{Na}$ .

| Transition  | $Q$ -value (MeV) | Effective matrix element $B_e$ |
|---|------------------|--------------------------------|
| $J^\pi(^{24}\text{Mg}) \rightarrow J^\pi(^{24}\text{Na})$ |                  |                                |
| $4^+ \rightarrow 2^+$                                     | 4.657            | $3.70 \times 10^{-8}$          |
| $1_1^+ \rightarrow 2^+$                                   | 5.129            | 0.0102                         |
| $2^+ \rightarrow 2^+$                                     | 5.220            | 0.0426                         |
| $1_1^+ \rightarrow 0^+$                                   | 6.498            | 0.0417                         |
| $1_2^+ \rightarrow 0^+$                                   | 7.373            | 0.461                          |

TABLE X. Numerical values of the quantities that determine the analytical expression for the electron capture rate on  $^{24}\text{Na}$ .

| Transition  | $Q$ -value (MeV) | Effective matrix element $B_e$ |
|---|------------------|--------------------------------|
| $J^\pi(^{24}\text{Na}) \rightarrow J^\pi(^{24}\text{Ne})$ |                  |                                |
| $1^+ \rightarrow 0^+$                                     | -2.505           | 0.118                          |
| $4^+ \rightarrow 4_1^+$                                   | -6.949           | $4.94 \times 10^{-3}$          |
| $4^+ \rightarrow 3_1^+$                                   | -7.794           | 0.301                          |
| $4^+ \rightarrow 3_2^+$                                   | -8.413           | 0.0753                         |
| $4^+ \rightarrow 4_2^+$                                   | -8.668           | 0.0390                         |

electron capture rates and increase the competing  $\beta$ -decay rates. This is visible in Fig. 10 where we compare the electron capture rate on  $^{24}\text{Mg}$  and the  $\beta$ -decay rate of  $^{24}\text{Na}$  calculated with and without the Coulomb corrections, applying the same formalism as discussed above for the case of the  $A = 20$  nuclei. As for the  $^{20}\text{Ne}$ - $^{20}\text{F}$  pair, the Coulomb corrections also shift the density at which the  $^{24}\text{Mg}$  capture and the  $^{24}\text{Na}$  decay rate become identical towards higher values, again by about 0.05 dex in  $\log(\rho Y_e)$ . We expect that this shift is a typical value for sd-shell nuclei at the conditions of the collapsing ONeMg core and should hence also affect the URCA pairs ( $^{23}\text{Na}$ - $^{23}\text{Ne}$ ,  $^{25}\text{Mg}$ - $^{25}\text{Na}$ ,  $^{27}\text{Al}$ - $^{27}\text{Mg}$ ) which play an important role for the cooling during the collapse [60].

In Fig. 11 we compare the medium-corrected rates for the  $A = 24$  nuclei and observe that electron capture on  $^{24}\text{Mg}$  dominates over  $^{24}\text{Na}$   $\beta$  decay for densities  $\log \rho Y_e > 9.3$ . However, at the astrophysical conditions at which the electron capture rate on  $^{24}\text{Mg}$  is larger than the competing  $^{24}\text{Na}$   $\beta$  decay, it is also larger than the capture rate on the daughter  $^{24}\text{Na}$ . The consequence is that once capture on  $^{24}\text{Mg}$  is faster than  $\beta$  decay it is followed by a second capture process leading to  $^{24}\text{Ne}$ .

In Fig. 12 we plot the quantity  $\mathcal{E}$  for electron capture on  $^{24}\text{Mg}$  and  $^{24}\text{Na}$  and for  $^{24}\text{Na}$   $\beta$  decay. The capture on  $^{24}\text{Mg}$  is endothermic up to about  $\log(\rho Y_e) = 9.3$ , while the capture process is exothermic at densities  $\rho Y_e > 10^9 \text{ g cm}^{-3}$ . Like for the  $A = 20$  nuclei this difference is due to pairing energy making the  $Q$  value for capture on  $^{24}\text{Mg}$  larger than for capture on  $^{24}\text{Na}$ . The  $^{24}\text{Na}$   $\beta$  decay is endothermic, explaining the negative values of  $\mathcal{E}$ . The kinks in  $\mathcal{E}$  occur when the rate is changing from the

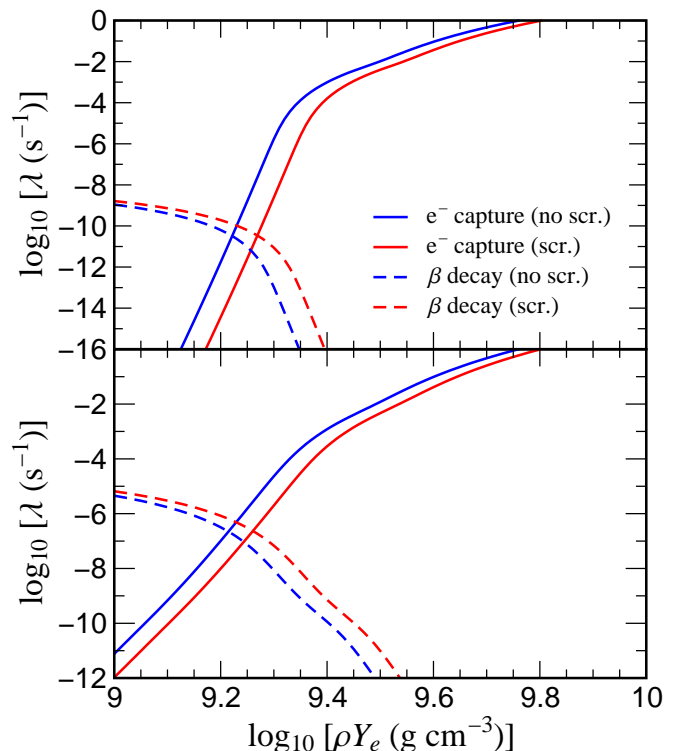


FIG. 10. Electron capture rate on  $^{24}\text{Mg}$  and beta decay rate of  $^{24}\text{Na}$  with and without consideration of medium corrections (upper panel:  $\log T(\text{K}) = 8.6$ , lower panel:  $\log T(\text{K}) = 9.0$ ).

dominance of one specific transition to another. The respective transitions are identified in our discussion of the individual rates. We observe good agreement with the results obtained by Takahara *et al.* [25] for the electron capture processes (these authors do not give results for the  $\beta$  decay). For densities  $\log(\rho Y_e) (\text{g cm}^{-3}) > 9.2$ , the energy produced by capture on  $^{24}\text{Mg}$  becomes positive. This together with the fact that capture on  $^{24}\text{Na}$  always produce energy for the conditions considered marks the transition density at which the net effect of the sequence of  $A = 24$  weak-interaction processes changes from endothermic to exothermic increasing the core temperature in stellar evolution models.

#### IV. CONCLUSION

We have calculated the rates for electron captures on  $^{20}\text{Ne}$ ,  $^{20}\text{F}$ ,  $^{24}\text{Mg}$ ,  $^{24}\text{Na}$  and  $\beta$  decays of  $^{20}\text{F}$  and  $^{24}\text{Na}$  which are key quantities for studies of the late-time evolution of 8–12  $M_\odot$  stars. So far such late-time studies are based on the rate evaluations of [25] and [5]. We have improved these rates in three important aspects. First, we have incorporated experimental data from either  $\beta$  decay or charge-exchange experiments which have not been available at the time when Takahara *et al.* [25] and Oda *et al.* [5] did their work. In our study the recent experimen-

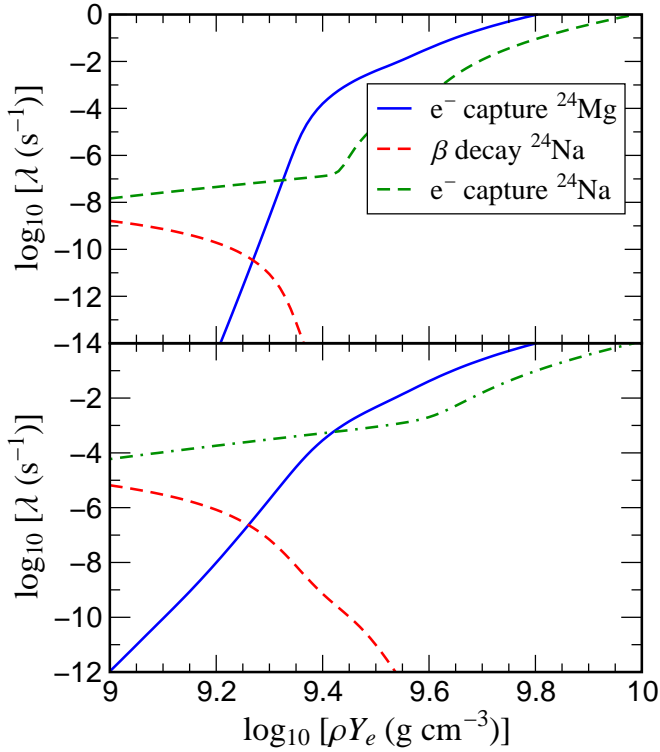


FIG. 11. Rates for electron captures on  $^{24}\text{Mg}$  and  $^{24}\text{Na}$  and beta-decay of  $^{24}\text{Na}$  for selected temperatures:  $\log T(\text{K}) = 8.6$  (upper panel),  $\log T(\text{K}) = 9.0$  (lower panel). Medium corrections are included in the rates.

tal data are supplemented by Gamow-Teller transitions derived from large-scale shell model calculations, similar to the procedure in [5, 25]. Importantly we find that nuclear physics input into the astrophysically relevant rates for electron captures on  $^{20}\text{Ne}$  and  $^{24}\text{Mg}$  and the competing beta decays of the respective daughters is completely based on experimental data. The exception is the electron capture on  $^{20}\text{Ne}$  in the density regime  $\log \rho Y_e = 9.3\text{--}9.7$ . As our second improvement we point out that at temperatures  $T < 0.7 \times 10^9$  the capture rate is likely to be dominated by the second-forbidden transition from the  $^{20}\text{Ne}$  ground state to the  $^{20}\text{F}$ . Experimentally only an upper limit exists, which, however, is of the order of typical second-forbidden transition strengths. While we have used the upper limit as an estimate for this transition in our present work a calculation of the transition with an appropriate method like the shell model or an experimental determination is highly desirable.

As the third improvement, we have corrected the various rates for medium-induced effects. Here we followed the formalism discussed in ref. [14] for electron captures and extended it to the treatment for  $\beta$ -decays. The environment reduces the electron chemical potential and enhances (reduces) the reaction  $Q$ -value for electron captures ( $\beta$  decays). As a consequence electron capture rates are lower in dense astrophysical environments than for bare nuclei, while  $\beta$  decay rates are larger. For the astro-

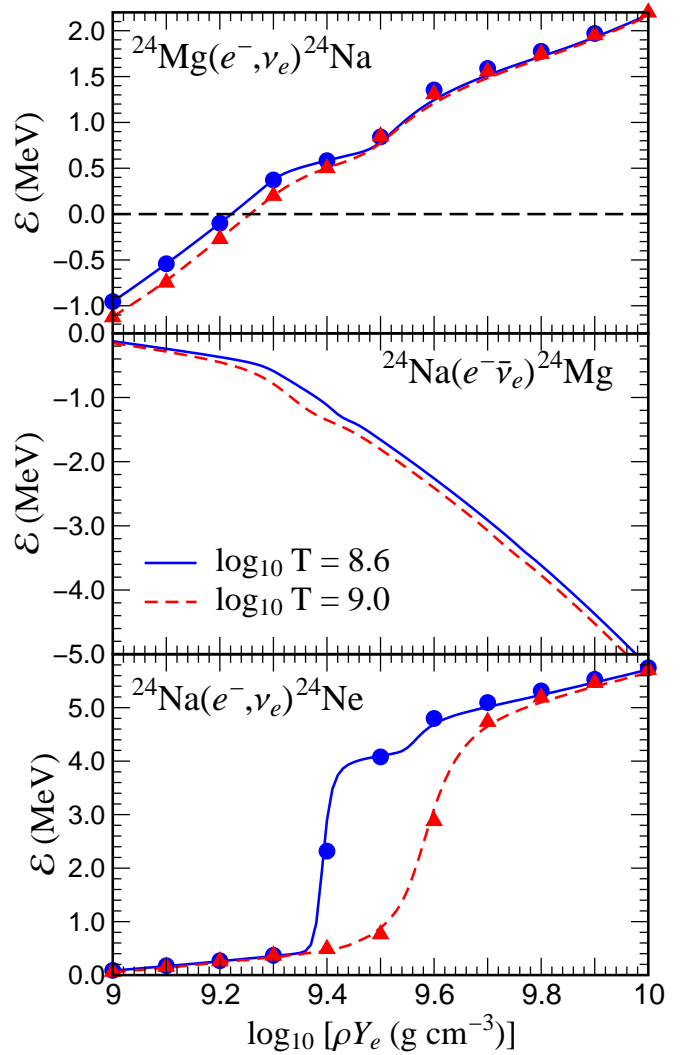


FIG. 12. Average energy produced (positive) or absorbed (negative) by electron capture on  $^{24}\text{Mg}$  (upper panel), beta-decay of  $^{24}\text{Na}$  (middle panel) and electron capture on  $^{24}\text{Na}$  (lower panel).

physical conditions here, the medium corrections change the rates typically by a factor of order two. The effect is, of course, significantly larger at such densities where the rates change from dominance of a certain transition to another (as is the case in the weak processes here) as these transitions are extremely sensitive to the effective  $Q$  values.

We note that medium effects should also have a significant effect on the densities at which so-called URCA pairs operate and influence the late-stage evolution of the stars. As  $\beta$  decay rates are enhanced and the competing electron capture rates are lowered, the medium modifications will move the operation of the URCA pairs to somewhat higher densities. As the shifts of the electron chemical potential and of the  $Q$  values are of order 100 keV under the relevant density (and temperature) conditions encountered, we expect that the URCA pairs

operate at densities which are about  $0.1 \times 10^9 \text{ g cm}^{-3}$  larger than found in calculations which do not consider medium corrections on the rate. Stellar evolution studies which investigate the impact of screening on the URCA pairs are needed.

We have presented analytical expressions for both electron capture and beta-decay rates that allow for an accurate description of these processes for conditions at which URCA pairs operate in both intermediate mass stars [33] and neutron stars [34].

Rate tables on fine grids in temperature and density in the ranges  $\rho Y_e = 10^8 - 10^{10} \text{ g cm}^{-3}$  and  $T = 10^8 - 10^{10} \text{ K}$  can be obtained by request from the authors.

## ACKNOWLEDGEMENTS

This work was supported by the ExtreMe Matter Institute EMMI in the framework of the Helmholtz Al-

liance HA216/EMMI, the Deutsche Forschungsgemeinschaft through contract SFB 634, the Helmholtz International Center for FAIR within the framework of the LOEWE program launched by the state of Hesse, the Helmholtz Association through the Nuclear Astrophysics Virtual Institute (VH-VI-417) and USNSF (PHY-1102511, PHY-0822648(JINA)). We thank B. A. Brown, T. Fischer, S. Jones, R. Hirschi, P. von Neumann-Cosel, and H. Schatz for fruitful discussions.

- 
- [1] H. A. Bethe, *Rev. Mod. Phys.* **62**, 801 (1990).
- [2] K. Langanke and G. Martínez-Pinedo, *Rev. Mod. Phys.* **75**, 819 (2003).
- [3] G. M. Fuller, W. A. Fowler, and M. J. Newman, *Astrophys. J. Suppl.* **42**, 447 (1980); *Astrophys. J. Suppl.* **48**, 279 (1982); *Astrophys. J.* **252**, 715 (1982).
- [4] G. M. Fuller, W. A. Fowler, and M. J. Newman, *Astrophys. J.* **293**, 1 (1985).
- [5] T. Oda, M. Hino, K. Muto, M. Takahara, and K. Sato, *At. Data Nucl. Data Tables* **56**, 231 (1994).
- [6] E. Caurier, K. Langanke, G. Martínez-Pinedo, and F. Nowacki, *Nucl. Phys. A* **653**, 439 (1999).
- [7] K. Langanke and G. Martínez-Pinedo, *Nucl. Phys. A* **673**, 481 (2000).
- [8] K. Langanke and G. Martínez-Pinedo, *At. Data. Nucl. Data Tables* **79**, 1 (2001).
- [9] D. Frekers, *Prog. Part. Nucl. Phys.* **57**, 217 (2006).
- [10] Y. Fujita, B. Rubio, and W. Gelletly, *Prog. Part. Nucl. Phys.* **66**, 549 (2011).
- [11] M. Sasano, G. Perdikakis, R. G. T. Zegers, S. M. Austin, D. Bazin, B. A. Brown, C. Caesar, A. L. Cole, J. M. Deaven, N. Ferrante, C. J. Guess, G. W. Hitt, R. Mehrarchand, F. Montes, J. Palardy, A. Prinke, L. A. Riley, H. Sakai, M. Scott, A. Stolz, L. Valdez, and K. Yako, *Phys. Rev. Lett.* **107**, 202501 (2011).
- [12] A. L. Cole, T. S. Anderson, R. G. T. Zegers, S. M. Austin, B. A. Brown, L. Valdez, S. Gupta, G. W. Hitt, and O. Fawwaz, *Phys. Rev. C* **86**, 015809 (2012).
- [13] H.-T. Janka, K. Langanke, A. Marek, G. Martínez-Pinedo, and B. Müller, *Phys. Repts.* **442**, 38 (2007).
- [14] A. Juodagalvis, K. Langanke, W. R. Hix, G. Martínez-Pinedo, and J. M. Sampaio, *Nucl. Phys. A* **848**, 454 (2010).
- [15] K. Langanke, G. Martínez-Pinedo, J. M. Sampaio, D. J. Dean, W. R. Hix, O. E. B. Messer, A. Mezzacappa, M. Liebendörfer, H.-T. Janka, and M. Rapp, *Phys. Rev. Lett.* **90**, 241102 (2003).
- [16] A. A. Dzhioev, A. I. Vdovin, V. Y. Ponomarev, J. Wambach, K. Langanke, and G. Martínez-Pinedo, *Phys. Rev. C* **81**, 015804 (2010).
- [17] N. Paar, G. Colò, E. Khan, and D. Vretenar, *Phys. Rev. C* **80**, 055801 (2009).
- [18] Y. F. Niu, N. Paar, D. Vretenar, and J. Meng, *Phys. Rev. C* **83**, 045807 (2011).
- [19] K. Nomoto, *Astrophys. J.* **277**, 791 (1984); *Astrophys. J.* **322**, 206 (1987).
- [20] W. Hillebrandt, K. Nomoto, and R. G. Wolff, *Astron. & Astrophys.* **133**, 175 (1984).
- [21] L. Hüdepohl, B. Müller, H. Janka, A. Marek, and G. G. Raffelt, *Phys. Rev. Lett.* **104**, 251101 (2010).
- [22] H. Ning, Y.-Z. Qian, and B. S. Meyer, *Astrophys. J.* **667**, L159 (2007).
- [23] H.-T. Janka, B. Müller, F. S. Kitaura, and R. Buras, *Astron. & Astrophys.* **485**, 199 (2008).
- [24] S. Jones, R. Hirschi, K. Nomoto, T. Fischer, F. X. Timmes, F. Herwig, B. Paxton, H. Toki, T. Suzuki, G. Martínez-Pinedo, Y. H. Lam, and M. G. Bertolli, *Astrophys. J.* **772**, 150 (2013).
- [25] M. Takahara, M. Hino, T. Oda, K. Muto, A. Wolters, P. Glaudemans, and K. Sato, *Nucl. Phys. A* **504**, 167 (1989).
- [26] J. C. Hardy and I. S. Towner, *Phys. Rev. C* **79**, 055502 (2009).
- [27] A. R. Edmonds, *Angular Momentum in Quantum Mechanics* (Princeton University Press, Princeton, New Jersey, 1960).
- [28] F. Osterfeld, *Rev. Mod. Phys.* **64**, 491 (1992).
- [29] B. A. Brown and B. H. Wildenthal, *Annu. Rev. Nucl. Part. Sci.* **38**, 29 (1988).
- [30] K. Langanke, D. J. Dean, P. B. Radha, Y. Alhassid, and S. E. Koonin, *Phys. Rev. C* **52**, 718 (1995).
- [31] G. Martínez-Pinedo, A. Poves, E. Caurier, and A. P. Zuker, *Phys. Rev. C* **53**, R2602 (1996).
- [32] A. Heger, K. Langanke, G. Martínez-Pinedo, and S. E. Woosley, *Phys. Rev. Lett.* **86**, 1678 (2001).
- [33] S. Tsuruta and A. G. W. Cameron, *Astrophys. Space Sci.* **7**, 374 (1970).

- [34] H. Schatz, S. Gupta, P. Möller, M. Beard, E. F. Brown, A. T. Deibel, L. R. Gasques, W. R. Hix, L. Keek, R. Lau, A. W. Steiner, and M. Wiescher, *Nature* **505**, 62 (2014).
- [35] M. Galassi, J. Davies, J. Theiler, B. Gough, G. Jungman, P. Alken, M. Booth, and F. Rossi, *GNU Scientific Library Reference Manual*, 3rd ed. (Network Theory Limited, United Kingdom, 2009).
- [36] J. M. Aparicio, *Astrophys. J. Suppl.* **117**, 627 (1998).
- [37] Z. Gong, L. Zejda, W. Däppen, and J. M. Aparicio, *Comp. Phys. Comm.* **136**, 294 (2001).
- [38] P. Haensel and J. L. Zdunik, *Astron. & Astrophys.* **404**, L33 (2003).
- [39] H. Bethe, G. Brown, J. Applegate, and J. Lattimer, *Nucl. Phys. A* **324**, 487 (1979).
- [40] S. L. Shapiro and S. A. Teukolsky, *Black Holes, White Dwarfs and Neutron Stars: The Physics of Compact Objects* (Wiley-Interscience, New York, 1983).
- [41] S. Gupta, E. F. Brown, H. Schatz, P. Möller, and K.-L. Kratz, *Astrophys. J.* **662**, 1188 (2007).
- [42] S. Miyaji, K. Nomoto, K. Yokoi, and D. Sugimoto, *Publ. Astron. Soc. Japan* **32**, 303 (1980).
- [43] K. Nakazawa, *Prog. Theor. Phys.* **49**, 1932 (1973).
- [44] B. D. Anderson, N. Tamimi, A. R. Baldwin, M. Elaasar, R. Madey, D. M. Manley, M. Mostajabodda'vati, J. W. Watson, W. M. Zhang, and C. C. Foster, *Phys. Rev. C* **43**, 50 (1991).
- [45] F. Ajzenberg-Selove, *Nucl. Phys. A* **475**, 1 (1987).
- [46] B. A. Brown and W. A. Richter, *Phys. Rev. C* **74**, 034315 (2006).
- [47] M. Wang, G. Audi, A. Wapstra, F. Kondev, M. MacCormick, X. Xu, and B. Pfeiffer, *Chinese Phys. C* **36**, 1603 (2012).
- [48] H. Behrens and W. Bühring, *Electron Radial Wave Functions and Nuclear Beta-decay* (Clarendon, Oxford, 1982).
- [49] P. von Neumann-Cosel, (2013), private communication.
- [50] D. Tilley, C. Cheves, J. Kelley, S. Raman, and H. Weller, *Nucl. Phys. A* **636**, 249 (1998).
- [51] E. Bravo and D. García-Senz, *Mon. Not. Roy. Ast. Soc.* **307**, 984 (1999).
- [52] N. Itoh, N. Tomizawa, M. Tamamura, S. Wanajo, and S. Nozawa, *Astrophys. J.* **579**, 380 (2002).
- [53] J. Gutiérrez, E. García-Berro, I. J. Iben, J. Isern, J. Labay, and R. Canal, *Astrophys. J.* **459**, 701 (1996).
- [54] D. Nishimura, Y. Fujita, M. Fukuda, E. Ganioglu, Y. Ichikawa, M. Kanazawa, A. Kitagawa, M. Mihara, S. Momota, B. Rubio, S. Sato, G. Susoy, M. Torikoshi, and K. Matsuta, *Eur. Phys. J. A* **47**, 1 (2011).
- [55] R. G. T. Zegers, R. Meharchand, T. Adachi, S. M. Austin, B. A. Brown, Y. Fujita, M. Fujiwara, C. J. Guess, H. Hashimoto, K. Hatanaka, M. E. Howard, H. Matsubara, K. Nakanishi, T. Ohta, H. Okamura, Y. Sakemi, Y. Shimbara, Y. Shimizu, C. Scholl, A. Signoracci, Y. Tameshige, A. Tamii, and M. Yosoi, *Phys. Rev. C* **78**, 014314 (2008).
- [56] M. E. Howard, R. G. T. Zegers, S. M. Austin, D. Bazin, B. A. Brown, A. L. Cole, B. Davids, M. Famiano, Y. Fujita, A. Gade, D. Galaviz, G. W. Hitt, M. Matos, S. D. Reitzner, C. Samanta, L. J. Schradin, Y. Shimbara, E. E. Smith, and C. Simenel, *Phys. Rev. C* **78**, 047302 (2008).
- [57] S. Rakers, C. Bäumer, D. Frekers, R. Schmidt, A. M. van den Berg, V. M. Hannen, M. N. Harakeh, M. A. de Huu, H. J. Wörtche, D. De Frenne, M. Hagemann, J. Heyse, E. Jacobs, and Y. Fujita, *Phys. Rev. C* **65**, 044323 (2002).
- [58] R. B. Firestone, *Nuclear Data Sheets* **108**, 2319 (2007).
- [59] D. E. Alburger, *Phys. Rev. C* **9**, 991 (1974).
- [60] H. Toki, T. Suzuki, K. Nomoto, S. Jones, and R. Hirschi, *Phys. Rev. C* **88**, 015806 (2013).